BOSTON UNIVERSITY

GRADUATE SCHOOL OF ARTS AND SCIENCES

DISSERTATION

KINETIC LATTICE MONTE CARLO AND AB INITIO STUDY OF POINT DEFECT MEDIATED DIFFUSION OF DOPANTS IN SILICON

by

MARIUS M. BUNEA

M.S., Bucharest University, 1991

Submitted in partial fulfillment of the

requirements for the degree of

Doctor of Philosophy

2000

Approved by

First Reader

Scott T. Dunham
Associate Professor of Electrical and Computer Engineering
University of Washington
Boston University

Second Reader

Karl Ludwig
Associate Professor of Physics
Boston University

Acknowledgments

First and foremost, I wish to thank my primary advisor Professor Scott T. Dunham for his boldness, direction and support in my doctoral work at Boston University. His deep understanding in the field of process and device modeling and his curiosity to learn more have kept us at the frontier of materials research. Professor Karl F. Ludwig's guidance and encouragements were a great help in my last year of graduate studies. I would like to thank my committee members Professors Scott Dunham, Karl Ludwig, Steven Ahlen, Roscoe Giles and Sidney Redner for their constructive comments related to my research. Many thanks also go to Dr. Wolfgang Windl and Dr. Roland Stumpf, from the Computational Material Group, Motorola Inc., who made ab-initio study of dopant diffusion in silicon a very illuminating experience for me. My colleagues in the process modeling group Mitra Navi, Srinivasan Chakravarti, Pavel Fastenko and Brendon Murphy have been good friends and have given me a great deal of support. I would like to acknowledge the Semiconductor Research Corporation whose financial support made this research project possible.

Lastly, I would like to express my love and gratitude to my parents who kept me focused and cultivated in me the curiosity for other cultures and horizons, to my big brother for his funny attitude and constant encouragements. My thanks also go to my wife whose love and support were a great inspiration.

KINETIC LATTICE MONTE CARLO AND AB INITIO STUDY OF POINT DEFECT MEDIATED DIFFUSION OF DOPANTS IN SILICON

(Order No.   )

MARIUS M. BUNEA

Boston University Graduate School of Arts and Sciences, 2000

Major Professor: Scott T. Dunham, Associate Professor of Electrical Engineering

ABSTRACT

Dopant diffusion in silicon has been studied for many years because of its importance in establishing dopant profiles in very large scale integrated devices, and because it is much more complicated than would be predicted by Fick's law. As electronic devices become smaller, understanding the atomistic mechanisms for dopant diffusion becomes crucial for the continued rapid advance in silicon technology.

In this work, dopant diffusion in silicon is studied using kinetic lattice Monte Carlo (KLMC) and ab initio calculations. A computer program has been written to investigate these phenomena. The KLMC approach is used to span the time and length scales between microscopic and macroscopic diffusion regimes. A model based on a lattice occupied by different particles (dopants, vacancies, interstitials, silicon atoms) with medium range interactions (up to tenth nearest neighbor) is employed with a range of boundary conditions. Hopping rates are based on changes in system energy and satisfy detailed balance. Different diffusion mechanisms are implemented. KLMC parameters (e.g. interactions energies) are obtained from experiment as well as ab-initio and empirical potential molecular dynamics calculations. The following problems were examined.

Vacancy mediated arsenic diffusion is found to increase dramatically in heavily doped silicon in agreement with experimental observations and previous calculations. However for very long simulation times arsenic diffusivity is reduced due to the formation of arsenic-vacancy complexes with clustering more pronounced at high concentration levels.

A dopant flux driven by a vacancy gradient is found to be smaller than, but in the same direction as, that predicted by a continuum diffusion model, the pair diffusion model, with the deviation greatest at high temperatures.

Simulated anneals of implant damage show that the long range vacancy-interstitial interaction as well as initial spatial correlations are important at low implant doses but are not important at high doses.

The potential use of the KLMC method is demonstrated for the study of very deep submicron devices via annealing of a 50nm channel length metal oxide silicon structure.

A new mechanism for B diffusion in silicon mediated by silicon self-interstitials is found via ab-initio calculations. The activation energy, migration barrier and diffusion length exponent are in good agreement with experiment.

Contents

List of Figures

List of Tables

List of Abbreviations

DFT	Density Functional theory
GGA	Gradient Generalized Approximation
KLMC	Kinetic lattice Monte Carlo
LDA	Local Density Approximation
MOS	Metal Oxide Semiconductor
MD	Molecular Dynamics
TED	Transient Enhanced Diffusion
TEM	Transmission Electron Microscopy

Chapter 1

Introduction

Dopant diffusion in silicon has been studied for many years because of its major technological importance as an elementary process step in fabrication of silicon-based integrated circuits. Dopant atoms are introduced into silicon substrates with the purpose of changing the electrical conductivity of the host material. These dopants then diffuse during some of the subsequent steps required to make electronic devices. Diffusion of dopants in silicon is more complicated than predicted by Fick's law, and for the last 30 years continuum models, based on solving coupled diffusion equations for dopants and point defects, have been the standard approach. Although computationally fast, they have become very complex and as such their predictions are uncertain.

A new trend is emerging in the study of dopant diffusion in silicon which consists in using experimental results and a broad range of numerical methods (e.g., first principle calculations, molecular dynamics (MD), kinetic lattice Monte Carlo (KLMC), coupled diffusion equations) to gain insight into the interactions of dopants with point defects. In this work, dopant diffusion in silicon was studied using kinetic lattice Monte Carlo and ab-initio calculations. The KLMC approach is used to span the time and length scales between microscopic and macroscopic regimes. A lattice model with different particles (dopants, vacancies, interstitials) with medium range interactions (up to tenth nearest neighbor) is employed with a range of boundary conditions. Hopping rates are based on changes in system energy and satisfy detailed balance. Different diffusion mechanisms (e.g., ring, kick out) are implemented. KLMC parameters (e.g., interactions energies) are obtained from both experiment as well as from ab-initio and empirical-potential MD calculations.

This first chapter provides an overview and introduction. The second chapter describes the native point defects, vacancies and silicon self-interstitials, which mediate dopant diffusion on silicon lattice. Also, thermodynamics of point defects are presented to show how relevant quantities like dopant defect interaction potential affect the number of point defects present in the lattice. Different diffusion mechanisms are also presented. Computational physics is the primary tool used in this work to investigate dopant diffusion in silicon. Kinetic Lattice Monte Carlo and ab initio pseudopotential calculations are presented in Chapter 3. In Chapter 4, the link between microscopic and macroscopic diffusion regimes is accomplished via kinetic lattice Monte Carlo, which also demonstrates the usefulness of this method. Chapter 5 presents another application of the KLMC method, anomalous diffusion of arsenic in silicon. The time dependence of diffusion is also investigated. The excess of silicon self interstitials following ion implantation is investigated in Chapter 6 as a function of interaction range, initial spatial correlations, implant energies and dose. According to the roadmap for semiconductors, in about 2012 the channel length of a MOS transistor will be 0.05 microns. For this very deep submicron transistor, atomic effects are critical and continuum modeling may be replaced by KLMC. An application of this method to the diffusion of an arsenic doped source and boron doped channel is presented in Chapter 7. A new diffusion mechanism for a the dominant p-type dopant in silicon, boron, identified via ab initio calculations is presented in Chapter 8. Finally, Chapter 9 summarizes the conclusions reached and suggests future work.

Chapter 2

Background

2.1 Point Defect Properties

2.1.1 Definition of Point Defects

Perfect crystals can be regarded as made of identical building blocks, unit cells, stacked in a repetitive array that defines the translational symmetry of the crystal structure. The crystal surface destroys the symmetry of the crystal, but its effects are neglected by definition in the study of bulk properties. While other extended defects are present in the crystal, point defects are of principal interest from the perspective of dopant diffusion in silicon. Two types of point defects may be identified: impurities and thermally activated point defects. Impurities are incorporated in silicon crystals from the growth process or in subsequent steps meant to introduce dopants that upon activation will change the electrical properties of silicon.

Thermally activated point defects or native point defects are present in the equilibrium structure of crystals at non-zero temperatures. Atomic motion associated with thermal energy causes atomic coordinates to fluctuate about their time average values and may have the effect of displacing the atoms from lattice sites into interstices where they may find new equilibrium positions as *interstitial* atoms. The empty site left behind when an interstitial is created is called a *vacancy* (see Fig. 2.1). This defect is also called a Schottky defect. A vacancy can exist in different charged states V^+, V^{++}, V^0, V^-, V^{--} (see Watkins *et al.* [1] for a complete study of vacancies in different charged states). For every charged state, the lattice presents a different distortion. These local distortions will be ignored in the lattice model that will be used to study diffusion. Only for a vacancy in the neighborhood of a dopant are they accounted for indirectly via the dopant-vacancy interaction potential. An interstitial is an atom transferred from a lattice site to a position not occupied by an atom in a perfect crystal. An interstitialcy is a region of the lattice which has an extra atom but for which one atom cannot be unambigously identified as the interstitial (e.g., two atoms sharing a lattice site). For this thesis we will use the term interstitial to include both interstitials and interstitialcies, making a distinction only if it is important. A dopant atom which resides on a lattice site is called a

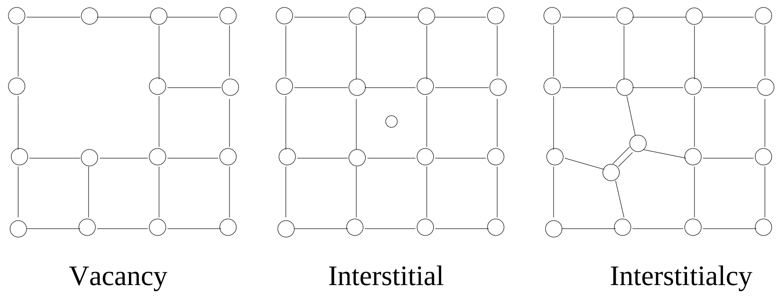

Figure 2.1: Native point defects of interest for silicon: vacancy — an empty lattice site, interstitial — an atom transfered from a lattice site to a position not occupied by an atom in the perfect crystal A dopant atom which is part of a region of the lattice with an extra atom is called a dopant interstitials or dopant interstitial pair. Both interstitial and interstitialcy will be called interstitial making a distinction only if it is important.

substitutional defect.

2.1.2 Why Study Point Defects?

Dopant atoms dissolve substitutionally in silicon. It is assumed that only by interacting with point defects, vacancies and interstitials, can dopant atoms perform long range diffusion. The diffusivity coefficient D_A for a dopant A under both equilibrium and nonequilibrium is given by the following equation:

$$D_A = D_A^{eq} \left[f_{AI} \frac{C_{AI}}{C_{AI}^{eq}} + f_{AV} \frac{C_{AV}}{C_{AV}^{eq}} + f_{ACE} \right] \tag{2.1}$$

By the superscript eq equilibrium conditions are implied. C_{AI} and C_{AV} represent the concentrations of migrating defects that allow diffusion of dopants, and f_{AI}, f_{AV} are experimentally found interstitial and vacancy mechanisms contribution to the dopant diffusion ($f_{AI} + f_{AV} + f_{ACE} = 1$). CE stands for the concerted exchange mechanism. Although the importance of the vacancy and interstitial mechanism for dopant diffusion is still debated, experiments suggest that P and B have the most substantial interstitial component of diffusion [2] ($f_{BI} = 0.84 - 1.0$, $f_{PI} = 0.86 - 1.00$), while Sb appears dominated by a vacancy mechanism [2] ($f_{SbI} = 0 - 0.16$). Oxidation of a silicon surface above an impurity doped layer leads to a large increase in the impurity diffusion above what is normally observed [2, 3]. At the same time extended defects — stacking faults — grow (see Fig. 2.2). TEM observation of stacking faults show that they are interstitial type defects. These defects grow by adding silicon atoms to the dislocation ends in oxidizing ambients. Hu [4] linked the growth of stacking faults and oxidation enhanced diffusion of dopants by proposing that they are due to silicon interstitials injected during oxidation. Under the same conditions, antimony diffusion is retarded which is explained through a decrease in the vacancy concentration due to recombination with interstitials and is evidence for a dominating vacancy mechanism for antimony diffusion.

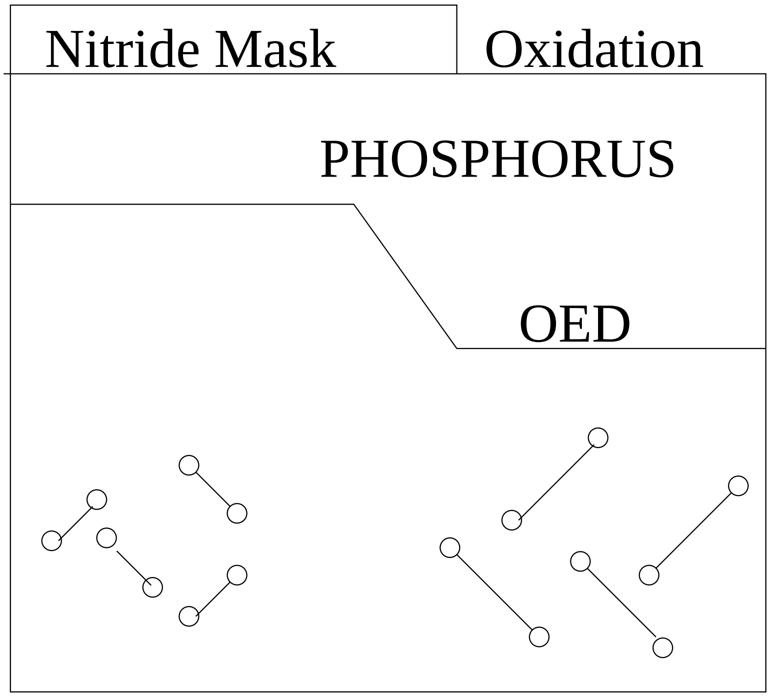

Figure 2.2: A schematic picture that shows the enhanced diffusion of phosphorus under the oxidizing region and the growth of stacking faults. Hu[4] proposed that the two phenomena have a common origin in the injection of silicon self interstitials. This type of experiment suggests that diffusion of impurities like P and B are dominated by an interstitial mechanism.

2.1.3 Thermodynamics of Point Defects

Why do point defects exist? Usually silicon wafers are kept at constant temperature and pressure. Under these conditions, the thermodynamical potential that is minimum at equilibrium is the Gibbs free energy:

$$G = H - TS \tag{2.2}$$

where H is the enthalpy, T is the absolute temperature, and S is the entropy. At any non-zero temperature, the silicon crystal will have a finite concentration of point defects, due to the fact that the energy cost for formation of a point defect is compensated by the entropy contribution. In this way the presence of point defects minimizes the free energy. Upon formation of a defect X (interstitial or vacancy), the change in the free energy is:

$$\Delta G_X = \Delta H_X^f - T\Delta S_X \tag{2.3}$$

ΔH_X^f is the enthalpy required to form a point defect X. The total entropy is the sum of three terms:

$$\Delta S_X = \Delta S_X^m + \Delta S_X^c + \Delta S_X^f \tag{2.4}$$

(mixing, configurational and formation entropies). The entropy of mixing depends on the number of different possible arrangements of point defects within the crystal and is defined as the difference in the entropy associated with the presence of n_X point defects versus n_{X-1}.

$$\Delta S_X^m = k\ln w(n_X) - k\ln w(n_X - 1) = k\ln\left[\frac{w(n_X)}{w(n_X - 1)}\right], \tag{2.5}$$

where $w(n_X)$ is the number of different possible arrangements of vacancies within the crystal. The configurational entropy, which depends on the number of different configurations of the vacancy θ_X is just:

$$\Delta S_X^c = k\ln\theta_X \tag{2.6}$$

The remaining entropy change is called the formation entropy ΔS_X^f, and is associated with changes in vibrational states with or without defects. At equilibrium $\Delta G_X = 0$

and substituting for the entropy terms we obtain:

$$\Delta H_X^f - T(\Delta S_X^m + \Delta S_X^c + \Delta S_X^f) = \Delta H_X^f - T\Delta S_X^f - kT\ln\left[\frac{\theta_X(C_s - C_X)}{C_X}\right], \quad (2.7)$$

where C_s is the concentration of sites and C_X is the concentration of defects. After some rearrangements and in the limit of dilute solutions($C_X \ll C_s$) we obtain:

$$C_X^* \simeq \theta_X C_s \exp\left[-\frac{\Delta G_X^f}{kT}\right], \quad (2.8)$$

where $\Delta G_X^f = \Delta H_X^f - T\Delta S_X^f$.

2.1.4 Nature of the Dopant Defect Interaction Potential

For analyzing dopant diffusion in silicon in the following chapters it will be useful to know how a dopant and a point defect interact. This interaction is described through an interaction potential and is calculated using quantum mechanics via first principle calculations which will be presented in the next chapter. There are two main contributions to the dopant-point defect interaction: Coulombic and elastic.

The dopant and the defect usually carry electric charge and as such a Coulombic potential between an ionized dopant atom and a charged point defect arises:

$$\Delta E_{Coul} = \frac{q_1 q_2}{4\pi\epsilon_0\epsilon_{Si} r} \quad (2.9)$$

where q_1 and q_2 are the charges on the two interacting particles, r the distance between them, and ϵ_{Si} is the macroscopic dielectric constant of Si (ϵ_{Si}=11.7). For close range interaction one performs more sophisticated corrections, finding the Madelung correction factor [5], in the previous equation. In Fig. 2.3 the dopant-vacancy interaction potentials from Pankratov *et al.* [5] and Nelson *et al.* [6, 7] are shown for As and P. Some distortion of the lattice must occur in order to accommodate

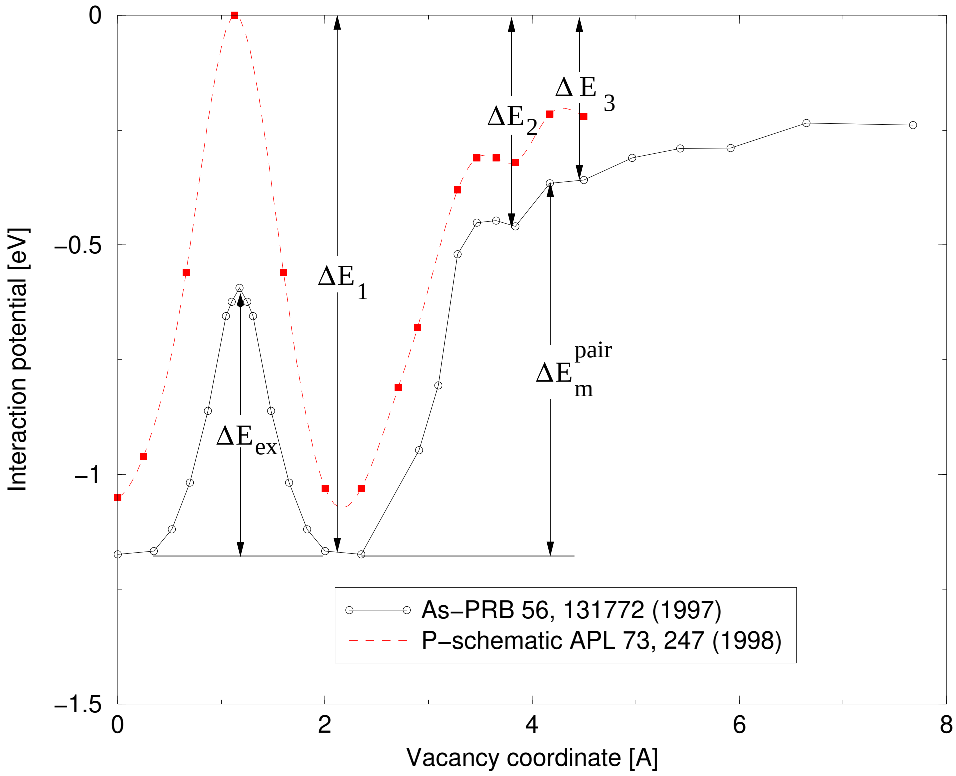

Figure 2.3: The As-vacancy and P-vacancy interaction potential [5, 6, 7]. The dopant atom is placed in the origin of the horizontal axis. The numbers on the horizontal axis enumerate lattice sites relative to the dopant atom. ΔE_{ex} is the energy barrier for the As atom to hop into the empty site (dopant-vacancy exchange), ΔE_1, ΔE_2 and ΔE_3 are the binding energies for the dopant-vacancy pair at first, second and third nearest neighbor, ΔE_m^{pair} is the migration barrier for the As-vacancy pair.

either native point defects or dopant atoms. Atoms with shorter bonding radii than silicon ($r_{Si} = 1.17$Å) are said to be "smaller" than silicon. Such dopants are P and B ($r_P = 1.1$Å, $r_B = 0.88$Å). All other dopants (Al, Ga, In, As, Sb and Bi) are "larger" than silicon ($r_A = 1.26, 1.26, 1.44, 1.18, 1.36, 1.45$Å) respectively. The size of the dopant atoms has a significant effect on the silicon lattice. Thus small atoms

Table 2.1: Si impurity bond lengths

Dopant	Calculated bond length	Sum of covalent radii
B	2.06	1.98
C	2.01	1.94
N	2.02	1.87
Al	2.39	2.42
Si	2.33	2.34
P	2.33	2.27
Sb	2.60	2.58

contract the lattice, big atoms dilate the silicon lattice. Nelson *et al.* [6, 7] have calculated the bond length for substitutional impurities and found that they follow the general trend of shorter bond lengths with atomic size (see Table 2.1). The bond lengths calculated are consistent with predictions based on a sum of covalent radii. The lattice relaxes inward for small atoms (B, C, N) and outward for big atoms (Al, Sb). As a result one finds smaller binding energy between a dopant with a inward relaxation and a vacancy, and a larger binding energy for a dopant with outward relaxation.

Self diffusion and dopant diffusion, as will be discussed at more length in the following chapters, can be described by an Arrhenius expression:

$$D = D_0 \mathrm{exp}(-Q/kT), \tag{2.10}$$

Experiments [3] find the activation energy Q for dopant diffusion to be 1 eV or more lower than self-diffusion. If one mechanism is dominant over the other then the activation energy for self diffusion is written as a sum of the defect formation enthalpy H_X^f and defect migration enthalpy H_X^m:

$$Q = H_X^f + H_X^m, \tag{2.11}$$

2.2 Atomistic Models for Point Defect Mediated Diffusion

2.2.1 Vacancy Mechanism

One way a substitutional dopant can diffuse through the lattice is by vacancy mechanism. This diffusion mechanism has been proposed for silicon based on the experimental observation that the vacancy is the main point defect in metals [8]. The vacancy mechanism can be well described as a succession of events:

1) pair formation;

2) pair as a random walker;

3) pair dissociation;

4) go back to step 1).

1) To understand pair formation, let us start with a case in which the empty site is located some distance away from the dopant (see Fig. 2.4). One of the four neighboring silicon atoms is going to hop into the empty site. The energy barriers however will not be the same. The attraction between dopant and vacancy will lower the energy barriers for the silicon atoms closer to the dopant atom such that the hopping frequencies $\nu_1 = \nu_4 > \nu_2 = \nu_3$. Gradually (on average) the empty site will move closer and closer to the dopant atom. When the dopant atom and the empty site are first nearest neighbors a pair is formed.

2) A schematic of the pair diffusion is shown in Fig. 2.5. At an atomistic scale, this mechanism presents some particularities given the different dopant-vacancy interactions. For As for instance, the vacancy mechanism does not occur through a simple dopant vacancy exchange, but through what is called “ring mechanism.” The vacancy not only must exchange its position with the dopant but also has to move away

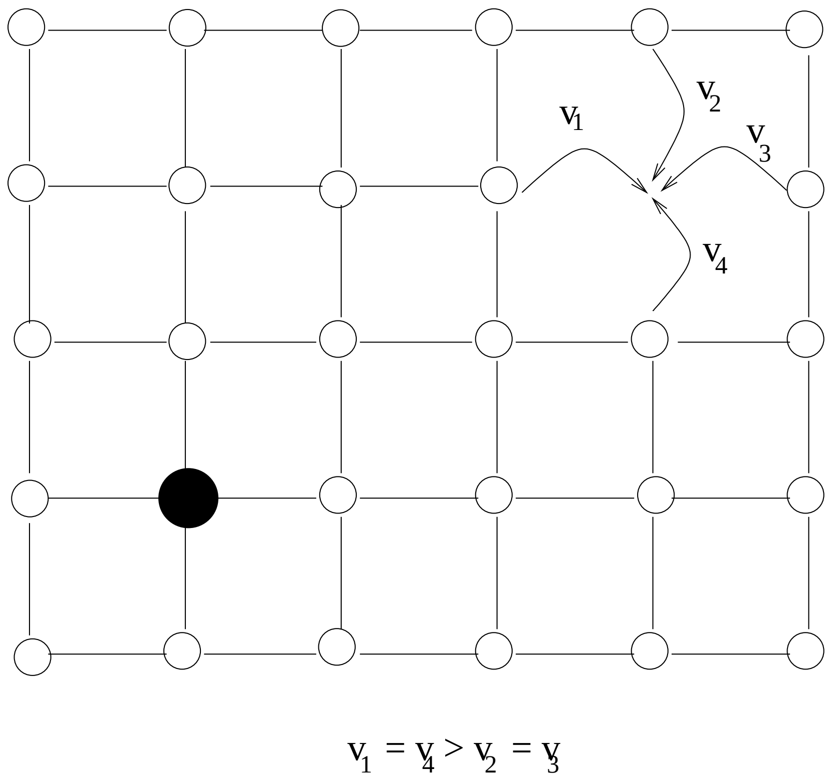

Figure 2.4: Dopant vacancy pair formation. Initially the empty site is located some distance from the dopant atom. One of the four neighboring silicon atoms is going to hop into the empty site. The energy barriers however will not be the same. The attraction between dopant and vacancy will lower the energy barriers for the silicon atoms closer to the dopant atom such that the hopping frequencies $\nu_1 = \nu_4 > \nu_2 = \nu_3$. Gradually the empty site will be located closer and closer to the dopant atom. When the dopant atom and the empty site are first nearest neighbors a pair is formed.

to a third nearest neighbor site with respect to the dopant and approach the dopant from a new direction for a long range migration of the dopant to take place. This mechanism is possible given the energy barriers associated with silicon or dopants atom hops onto the empty sites that are calculated by quantum mechanics via first principle calculations.

The activation energy is usually written for dopant diffusion as the sum of the

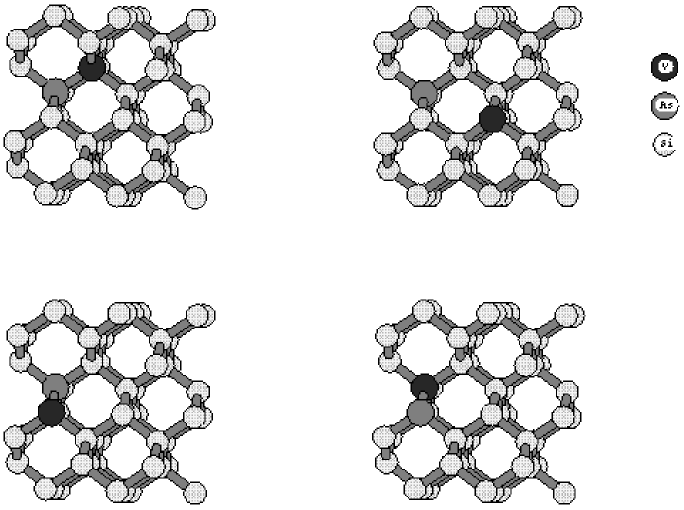

Figure 2.5: The dopant vacancy pair migration on the silicon lattice. In the upper left figure, the dopant (gray) and the vacancy (shown as a dark particle) are first nearest neighbors. The hopping rates are such that the dopant can hop into the empty site and back many times without any effect on diffusion. The host atoms, though, could also hop into the empty site such that at some point the vacancy moves to a third nearest neighbor site with respect to the dopant as in the upper right figure. Then the vacancy can go around the six member ring of atoms and approach the dopant from a different direction as in the lower left figure. Following another hop of the dopant into the empty site, as in the lower right figure, the dopant vacancy pair has performed one step as a random walker.

pair formation energy H^f_{AV} and and the pair migration energy H^m_{AV},

$$Q = H^f_{AV} + H^m_{AV}, \tag{2.12}$$

where the formation enthalpy of the pair $H^f_{AV} = H^f_V - E^b_{AV}$ and E^b_{AV} is the binding energy of the AV pair. For other dopants like P the limiting step is not the vacancy reaching the third nearest neighbor site with respect to the dopant but dopant vacancy exchange (see Fig. 2.3).

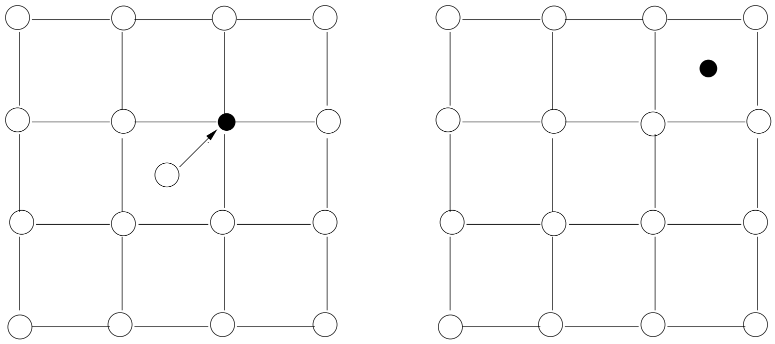

Figure 2.6: Dopant diffusion via interstitial mechanism. The dark atom is a substitutional dopant. A silicon self interstitial hopping through the interstices of the silicon lattice approaches the substitutional dopant and the energy barrier is low enough that the dopant is kicked out of its site into an interstices and then migrates through the interstices of the Si lattice until it kicks out a host atom and becomes substitutional again.

2.2.2 Interstitial Mechanism

In this mechanism, a silicon interstitial migrates through the interstices of the lattice and approaches a substitutional atom. If the energy barrier is low, the substitutional dopant becomes an interstitial atom and could migrate through the lattice as a dopant interstitial. This process is described by the reaction:

$$A_s + I \Leftrightarrow A_i, \tag{2.13}$$

An example of the interstitial mechanism is shown in Fig. 2.6.

More recent calculations [9, 10] find that after a boron silicon self-interstitial pair is formed, the boron atom kick-out into a hexagonal position. Instead of hopping into another hexagonal position via a tetrahedral site as saddle point as in the previous calculations [11], more likely boron kicks back in as a substitutional atom.

Chapter 3

Numerical Methods Employed

3.1 Kinetic Lattice Monte Carlo

For deep submicron devices the discrete nature of the system and the corresponding atomic scale behavior are important. Kinetic Lattice Monte Carlo has emerged as an effective method for extending atomistic simulations to time accessible by experiments. There are two reasons for this. On one hand, the fundamental time step in KLMC is related to hops (the time between $10^{-9} - 10^{-6}$ s) rather than the vibration period ($10^{-14} - 10^{-13}$ s) as in molecular dynamics simulations. On the other hand, the method considers only dopants and defects present in the system ($10^{10} - 10^{21}\mathrm{cm}^{-3}$), which is much smaller than the atom density ($5 \times 10^{22}\mathrm{cm}^{-3}$). Also as the devices become smaller continuum models become more complex, while LMC computational requirements scale with L^3 and are inherently 3D.

3.1.1 Statistical Mechanics of KLMC

In the lattice model underlying KLMC, it is assumed that atoms oscillate with small amplitudes about fixed sites, at high temperatures at which diffusion usually takes place, and now and then hop to available sites if such sites are first nearest neighbors. The classical Hamiltonian contains a kinetic and a potential term [12]:

$$H(\vec{p},\vec{r}) = T(\vec{p}) + V(\vec{r}) \tag{3.1}$$

such that the probability density of finding the system in the neighborhood of a phase space point ($\vec{p}$,$\vec{r}$) is :

$$P(\vec{p},\vec{r}) = \frac{1}{Z}\exp(-\beta H(\vec{p},\vec{r})), \tag{3.2}$$

where $\beta = 1/k_BT$, k_B is Boltzmann's constant and T is the absolute temperature. Z is the partition function and has the value:

$$Z = \int d\,\vec{p} \int d\,\vec{p}\,\exp(-\beta H(\vec{p},\vec{r})) \tag{3.3}$$

In the Monte Carlo method the momenta of the atoms are neglected. Integrating over momenta one obtains the probability density of having the system in the neighborhood of some set of spatial coordinates:

$$P(\vec{r}) = \frac{1}{Z}\exp(-\beta V(\vec{r})) \tag{3.4}$$

Now we introduce the harmonic approximation for the potential energy V($\vec{r}$). The set of sites about which atoms vibrate are $\vec{R_i}$ for some configuration i. When the atoms occupy these sites the local energy is minimum and the atoms experience no force. The net displacements from these sites is given by $\vec{u}$, $\vec{r}$=$\vec{R_i}$ + $\vec{u}$. Within the harmonic approximation the potential energy can be written as:

$$V(\vec{r}) \approx V(\vec{R_i}) + \frac{1}{2}\,\vec{u}\,\mathbf{D_i}\,\vec{u} \tag{3.5}$$

The integral over $\vec{r}$ is replaced with a sum over i and and integral over $\vec{u}$. Assuming that the dynamical matrix is independent of configuration and integrating over $\vec{u}$, we get the probability of the system to be in the configuration i:

$$P(\vec{R_i}) = \frac{\exp(-\beta V(\vec{R_i}))}{\sum_j \exp - \beta V(\vec{R_j})} \tag{3.6}$$

If the dynamical matrix changes between states, the last equation can be generalized by replacing $V(\vec{R_i})$ with $V(\vec{R_i}) + \frac{1}{2}\vec{u}\,\mathbf{D_i}\,\vec{u}$.

3.1.2 Kinetics of KLMC

Transition from one state to another is governed by the Markovian master equation [13]:

$$\frac{\partial P_i}{\partial t} = -P_i W_{ij} + \sum_j P_j W_{ji} \tag{3.7}$$

where P_i is the probability of finding the system in a state i, W_{ij} is the rate of going from a state i into another state j. At local equilibrium detailed balance holds:

$$P_i W_{ij} = P_j W_{ji} \tag{3.8}$$

Combining equations (3.6) and (3.8) we obtain:

$$\frac{W_{ij}}{W_{ji}} = \exp(-\beta(V(\vec{R_j}) - V(\vec{R_i}))) \tag{3.9}$$

The transition rates from one state to another are taken from calculations or experiment where available. When no information is available, they are postulated to be:

$$W_{ij} = W_0 \exp\left(-\frac{\beta}{2}\left[V(\vec{R_j}) - V(\vec{R_i})\right]\right) \tag{3.10}$$

where W_0 corresponds to the most closely-related transition whose rate is known.

To find the potential energy corresponding to different configurations in Equation (3.10), for which calculated or experimental values are not available, a variety of approaches are possible. One example is the lattice gas theory applied to a binary alloy [14] where the lattice is populated with different types of atoms, say 1 and 2, with the numbers of nearest neighbors being N_{11}, N_{22}, N_{12} such that the configuration energy could be written as:

$$E = \epsilon_{11}N_{11} + \epsilon_{22}N_{22} + \epsilon_{12}N_{12}, \tag{3.11}$$

where ϵ_{11}, ϵ_{22} and ϵ_{12} denote the interaction energies of the different types of pairs. The number of particles could be kept constant as in Kawasaki models [15], or could change during the evolution of the system like in Glauber models [15]. Long range interactions up to tenth nearest neighbor are taken into account with binding energies assumed to be additive. Also energy look-up tables have been implemented for a more general framework.

In this work a lattice model is used where each site is either empty or occupied by a host atom or a dopant atom or both. The vacant site will be treated simply as another species. Mobile species are vacancies, interstitials and dopant interstitials. In the course of simulations, hopping rates are calculated for all mobile species in the system, taking into account only hops to first nearest neighbor sites. At each step, a hop is chosen randomly, weighted by the relative rates. The time is incremented by an amount given by the inverse sum of rates:

$$\Delta t = \left[\sum_{i=1}^{N} \sum_{i=j}^{4} \nu_{ij} \right]^{-1}, \tag{3.12}$$

where N is the number of mobile species in the system and the second sum accounts for the four possible hop directions. Hopping rates are recalculated in the neighborhood of the hop which just occurred and a new hop is chosen, advancing the system in time.

3.2 Ab Initio Pseudopotential Calculations

3.2.1 Introduction to the Pseudopotential Method

In solving the Schrödinger equation for solids, space can be divided into two regions with quite different properties. The regions near nuclei, the "core regions," are composed of tightly bound electrons which respond very little to the presence of neighboring atoms, while the remaining volume contains the valence electron density which are involved in the bonding together of the atoms. Although the potential in the core is strongly attractive for valence electrons, the requirement that valence electrons states be orthogonal to those of the core produces a large kinetic energy which contributes an effective repulsive potential for the valence states. The valence electrons are responsible for the main properties of solids. To find the eigenstates and eigenvalues of these valence electrons one needs to solve the Schrödinger equation. We obtain the same valence eigenfunctions and eigenvalues if we work with a "pseudopotential" (which inside the core is very weak and produces a nodeless "pseudofunction") identical with the real potential outside the core, as long as the "pseudofunction" produces the same boundary condition at the core radius r_c as the real eigenfunction. In this way, the valence electrons “do not know” that something was changed in the core region.

The pseudopotential approach represents a major achievement in band structure calculation. Usually in band structure calculation one deals with difficult questions related to self-consistent crystal potentials which very often obscure the underlying physical features. By contrast the pseudopotential method avoids these difficulties at very little, if any, cost in accuracy. One area of application for pseudopotential method is the study of energetics of point defects.

The pseudopotential method grew out of the orthogonalized plane wave (OPW) method, in which wave functions were expanded in a set of plane waves (PW) which are orthogonalized to all of the core wavefunctions $|\Psi_c\rangle$ [17]:

$$|\mathrm{OPW},K\rangle = |\mathrm{PW},K\rangle - \sum_{c}^{core} |\Psi_c\rangle\langle\Psi_c|\mathrm{PW},K\rangle \tag{3.13}$$

where the wavevector K labels the PW or OPW. The construction of a pseudopotential can be demonstrated in terms of the exact core and valence states $|\Psi_c\rangle$, $|\Psi_v\rangle$ which satisfy:

$$H|\Psi_i\rangle = E_i|\Psi_i\rangle, \qquad i = c, v \tag{3.14}$$

We can substract the core orthogonality oscillations to obtain the pseudostates $|\Phi_v\rangle$ given by:

$$|\Phi_v\rangle = |\Psi_v\rangle + \sum_c |\Psi_c\rangle\alpha_{cv}, \tag{3.15}$$

with $\alpha_{cv} = \langle\Psi_c|\Phi_v\rangle$. Applying H to $|\Phi_v\rangle$ gives:

$$H|\Phi_v\rangle = E_v|\Psi_v\rangle + \sum_c E_c|\Psi_c\rangle\alpha_{cv} = E_v|\Phi_v\rangle + \sum_c (E_c - E_v)|\Psi_c\rangle\alpha_{cv} \tag{3.16}$$

or

$$\left\{ H + \sum_c (E_v - E_c)|\Psi_c\rangle\langle\Psi_c| \right\} |\Phi_v\rangle = E_v|\phi_v\rangle. \tag{3.17}$$

Thus the valence pseudostates $|\Phi_v\rangle$ satisfy a Schrödinger equation with an energy-dependent pseudo-Hamiltonian:

$$H^{ps}(E) = H + \sum_c (E - E_c)|\Psi_c\rangle\langle\Psi_c| \tag{3.18}$$

3.2.2 Density Functional Theory

A periodic system is considered with atoms at positions $\mathbf{R} + \tau$,where $\mathbf{R}$ is a Bravais lattice vector locating a unit cell of the crystal and τ is a basis vector giving the positions in the unit cell. The Hamiltonian of the system is given by:

$$H = -\sum_{i=1}^{N} \frac{1}{2m}\nabla_i^2 + \sum_{i=1}^{N} V_{ion}(\mathbf{r_i}) + \frac{1}{2}\sum_{i \neq j}^{N} v(\mathbf{r_i} - \mathbf{r_j}) + V_{I-I} \tag{3.19}$$

which describes N electrons at positions $\mathbf{r_i}$ interacting via the Coulomb potential $v(\mathbf{r}) = e^2/|\mathbf{r}|$ and moving in the potential of the static ions given by:

$$V_{ion}(\mathbf{r}) = \sum_{m,s} V_{ion}^{(s)}(\mathbf{r} - \mathbf{R_m} - \tau_\mathbf{s}) \tag{3.20}$$

The ion-ion repulsion is given by:

$$V_{I-I} = \frac{1}{2} \sum_{mm^{'}ss^{'}}^{'} \frac{Z_s Z_{s^{'}} e^2}{|\mathbf{R_m} + \tau_\mathbf{s} - \mathbf{R_{m^{'}}} - \tau_{\mathbf{s}^{'}}|} \tag{3.21}$$

where the $m = m^{'}$, $s = s^{'}$ is to be omitted from the summation. In this chapter Rydberg atomic units ($\hbar = 1$, $2m = 1$, $e^2 = 2$) will be used, distances being measured in Bohr units and energies in Rydberg. The first three terms in eq. 3.18 could be lumped together as the electron energy operator H^{el}. A central result in DFT is that the ground state electronic energy E^{el} of the system is given by:

$$E^{el} = T_0[n] + \int V_{ion}(\mathbf{r})n(\mathbf{r})\mathrm{d}\mathbf{r} + E_h[n] + +E_{xc}[n], \tag{3.22}$$

where $T_0[n]$ is the kinetic energy of a system of non-interacting electrons with density $n(\mathbf{r})$, E_h is the classical interaction energy:

$$E_h(n) = \frac{1}{2}\int\int n(\mathbf{r})v(\mathbf{r}-\mathbf{r}^{'})n(\mathbf{r}^{'})\mathrm{d}\mathbf{r}\mathrm{d}\mathbf{r}^{'} \tag{3.23}$$

and E_{xc} is the exchange-correlation energy, which is a functional of n.
E^{el} can then be minimized with respect to density:

$$\left.\frac{\delta E^{el}[n]}{\delta n(\mathbf{r})}\right|_{n=n_0} = \mu \tag{3.24}$$

where μ is the chemical potential of the electronic system. The last equation is satisfied if the following set of Kohn-Sham equations is solved self-consistently:

$$h\Psi_i(\mathbf{r}) = \left\{-\frac{1}{2m}\nabla^2 + V_{eff}(\mathbf{r};n)\right\}\Psi_i(\mathbf{r}) = \epsilon_i\Psi_i(\mathbf{r}) \tag{3.25}$$

$$V_{eff}(\mathbf{r};n) = V_{ion}(\mathbf{r}) + V_h(\mathbf{r};n) + V_{xc}(\mathbf{r};n) \tag{3.26}$$

$$n(\mathbf{r}) = \sum_{i=1}^{N}|\Psi_i(\mathbf{r})|^2 \tag{3.27}$$

Here $\{\Psi_i\}$ and $\{\epsilon_i\}$ are the orthonormal eigenfunctions and the eigenvalues of the one-electron Hamiltonian h. The Hartree and exchange-correlation (XC) potentials are given by:

$$V_h(\mathbf{r};n) = \int v(\mathbf{r} - \mathbf{r}\prime)n(\mathbf{r}\prime)\mathrm{d}\mathbf{r}\prime \tag{3.28}$$

$$V_{xc}(\mathbf{r};n) = \frac{\delta E_{xc}[n]}{\delta n(\mathbf{r})}. \tag{3.29}$$

Ψ_i and ϵ_i resemble the excited wavefunctions and energies of the many body systems.

3.2.3 Local Density Approximation

The success of the density functional theory would not have been possible if not for an approximation related to the exchange-correlation of the electronic system called the local density approximation. In this approximation, it is assumed that the exchange-correlation energy per electron at point $\mathbf{r}$ in the electron gas $\epsilon_{xc}(\mathbf{r})$ is the same as the exchange-correlation energy per electron in a homogeneous electron gas that has the same density as the electron gas at point $\mathbf{r}$:

$$\epsilon_{xc}(\mathbf{r}) = \epsilon_{xc}^{hom}[n(\mathbf{r})] \tag{3.30}$$

with

$$E_{xc}[n(\mathbf{r})] = \int \epsilon_{xc}(\mathbf{r})n(\mathbf{r})d\mathbf{r} \tag{3.31}$$

3.3 Nudged Elastic Band Method

An important problem in diffusion processes in solids is the identification of the lowest energy path for a rearrangement of a group of atoms from one stable configuration to another [18]. The potential energy maximum along such a path is the saddle point energy which gives the activation energy barrier, a quantity of central importance in our kinetic lattice Monte Carlo studies of impurity diffusion in silicon.

Widely used methods for finding reaction paths and saddle points make use of two point boundary conditions, where both the initial and the final configurations for the transition are given. They are usually two local minima on the multidimensional potential energy surface which may be obtained by Monte Carlo simulated annealing methods or molecular dynamics. A chain of states (or images) of the system is generated between the end point configurations and all the intermediate images are optimized simultaneously.

In the so called "chain of states methods" several images are connected together to form a path, and an object function is minimized with respect to the intermediate images to find the lowest energy path. One example of such a function in the space of configurations connected via springs is:

$$S(\vec{R}_1, \vec{R}_2 \ .... \ \vec{R}_{P-1}) = \sum_{i=0}^{P} V(\vec{R}_i) + \sum_{i=1}^{P} \frac{Pk}{2}(\vec{R}_i - \vec{R}_{i-1})^2, \tag{3.32}$$

where $V(\vec{R}_i)$ is a potential function associated with a given configuration. The second term in the above equation is the elastic energy associated with a spring connecting images i and j, where k is the spring constant. The end points R_0 and R_P are kept fixed. This method is called the elastic band method.

There are usually two problems with the elastic band method. The force acting on image i is:

$$\vec{F}_i = -\vec{\nabla} V(\vec{R}_i) + \vec{F}_i^s \tag{3.33}$$

where

$$\vec{F}_i^s = k_{i+1}(\vec{R}_{i+1} - \vec{R}_i) - k_i(\vec{R}_i - \vec{R}_{i-1}). \tag{3.34}$$

For a larger value of k (e.g. $k = 1$) the elastic band is too stiff and cuts the corner and misses the saddle point. For a smaller value of k (e.g. $k = 0.1$) the images slide down and avoid the barrier region, reducing the resolution of the path in the critical region. The solution to the above problems in the nudged elastic band method is to project out the perpendicular component of the spring force and the parallel component of the true force, such that the force on image i becomes:

$$\vec{F}_i^0 = -\vec{\nabla} V(\vec{R}_i)|_\perp + \vec{F}_i^s \vec{\tau}_\| \vec{\tau}_\|, \tag{3.35}$$

where $\vec{\tau}_\|$ is the unit tangent to the path. These force projections decouple the dynamics of the path from the particular distribution of images chosen in the representation of the path, thus ensuring convergence of the lowest energy path.

Chapter 4

Corrections to Continuum Models

4.1 Corrections to the pair diffusion model

A central question in understanding dopant diffusion is how to relate the macroscopic diffusion behavior to the microscopic processes involving interactions between individual particles. For a strong dopant-vacancy binding energy, as shown in Fig. 2.2, migration of dopant-vacancy pairs occurs. The “pair diffusion” model [19, 20], as also described by Eq. 2.11, is currently the standard approach used in continuum simulators [3]. Previous work [21] studied the validity of this model and that of an alternative “non Fickian diffusion” model [22, 23] by taking into account a variety of assumed dopant-vacancy interaction potentials. It was found that for an attractive potential the dopant flux is in the same direction as the vacancy flux (in favor of the pair diffusion model), and is dependent on the difference between activation energy of the dopant diffusivity and that of tracer diffusion.

In this work the direction and the magnitude of a dopant flux in a vacancy gradient is studied for two substitutional dopants, As and P, and related to their diffusion via a vacancy mechanism in silicon at moderate doping levels. A lattice model is used with transition rates based on recent first-principle calculations [5, 6, 7] for dopant-vacancy interaction up to third nearest neighbor distance (4.5 Å) for P and sixth nearest neighbor (6.65 Å) for As. Results over a range of temperatures are compared to the pair diffusion model.

Two approaches can be used to relate the flux of dopants driven by a gradient of vacancies when a local thermodynamic equilibrium is assumed. In a first, more general approach [21, 24] following Onsager's [25] linearized nonequilibrium transport theory, the dopant flux is described by the following equation:

$$J_A = -\Lambda_{AA}\nabla\mu_A - \Lambda_{AV}\nabla\mu_V, \tag{4.1}$$

where Λ_{AA} and Λ_{AV} are the Onsager coefficients and μ_A, μ_V are the chemical potentials of dopants and vacancies. Writing the chemical potentials as functions of particle concentrations C_A, C_V for low concentrations one obtains:

$$J_A = -D_{AA}\nabla C_A - D_{AV}\nabla C_V, \tag{4.2}$$

where D_{AA} is the effective diffusion coefficient of dopant and D_{AV} accounts for the flux of dopant driven by a vacancy gradient.

A second approach, based on the pair diffusion model, finds a similar expression from Fick's first law and the mass action law ($C_{AV} = K_{AV}C_AC_V$) for the reaction of a substitutional dopant and a vacancy [19, 20]:

$$J_A = -K_{AV}d_{AV}[C_V\nabla C_A + C_A\nabla C_V], \tag{4.3}$$

where C_A and C_V are dopant and vacancy densities, and d_{AV} is the pair diffusivity. See Appendix A for a proof.

This expression is widely used in process simulators [26]. To quantify the results of this work, Equation (3) is modified to include a correction factor γ:

$$J_A = -K_{AV} d_{AV} [C_V \nabla C_A + \gamma C_A \nabla C_V]. \tag{4.4}$$

Comparing Equations (2) and (4), $D_{AA} = K_{AV} d_{AV} C_V$ and $D_{AV} = \gamma K_{AV} d_{AV} C_A$. In the pair diffusion model γ is assumed to be 1. In this work, γ is calculated by performing kinetic lattice Monte Carlo (KLMC) simulations [27, 28, 29, 30] with ab initio dopant-vacancy interactions based on LDA results [5, 6, 7] (Table 4.1). The ab initio method employed is described in references [27, 28, 29, 30].

The dopant vacancy pair is treated as neutral, with the dopant A in positively charged state and the vacancy in a negatively charged state, as is the case for moderately to heavily As or P doped silicon due to the linear dependence of the diffusivity on n/n_i, where n and n_i are the electron concentrations under extrinsic and intrinsic doping conditions. Simulations were initiated by placing one dopant and one vacancy randomly on a silicon lattice. At each step the vacancy exchanges its site with a dopant atom or a silicon atom. Only hops to first nearest neighbor sites are considered. Transition rates satisfy detailed balance and are postulated to be:

$$\nu = \nu_m \exp\left[\frac{E_i - E_f}{2k_B T}\right], \tag{4.5}$$

where $E_i - E_f$ is the change in the system energy associated with a possible hop, k_B is Boltzmann's constant, and T is the absolute temperature. The correction factor γ is the same if different transition rates based on ab initio saddle points [31] are used. Details of the KLMC method are described more fully in Section 3.1.

For exchanges with silicon atoms, the value of ν_m associated with vacancy hops

Table 4.1: Exchange energy barrier and binding energies up to sixth nearest neighbor for As-vacancy and up to third nearest neighbor for P-vacancy from recent ab initio calculations[5, 6, 7]. All energies are given in eV.

Dopant	E_{exch}	E_b^1	E_b^2	E_b^3	E_b^4	E_b^5	E_b^6
As	0.58	1.17	0.46	0.36	0.29	0.29	0.23
P	1.05	1.05	0.59	0.47			

is chosen such that the diffusivity of vacancies in pure silicon (D_v=0.125νa^2) is $D_v = 1.18 \times 10^{-4}\exp(-0.2\text{eV}/k_BT)$ cm^2/sec, where 0.2 eV is the migration enthalpy as obtained from ab initio calculations [7] and the prefactor (which does not affect the calculation of the correction factor γ) is from tight binding molecular dynamics calculations [16]. Ab initio calculations [6] have an error of about 0.1 eV for migration enthalpy and experimental values [1] are between 0.18 eV and 0.45 eV for the vacancy in different charged states. A value of 0.2 eV has been used because it was obtained by the same method as the one that found the exchange and binding energies. Thus the parameters used are a self consistent set. Tests with migration enthalpies between 0.1 eV and 0.3 eV found the same value (error less than 2% for the correction factor γ. For dopant-vacancy exchange, the migration enthalpy in ν_m is changed to match the calculated exchange barriers (Table 4.1). Note that a very large exchange barrier is calculated for P, such that P-V exchange, rather than separation to third-nearest neighbor distance is the rate limiting step for diffusion [29].

The vacancy gradient is implemented by adding a bias to vacancy transition rates between the bottom ($z = N_z - 1$) and top ($z = 0$) of the simulation cell.

$$\nu(1 \rightleftharpoons 2) = \nu\exp(\pm b) \tag{4.6}$$

Otherwise periodic boundary conditions are imposed. In Fig. 4.1 we see that the probability to find the vacancy on one of the (001) planes perpendicular to the

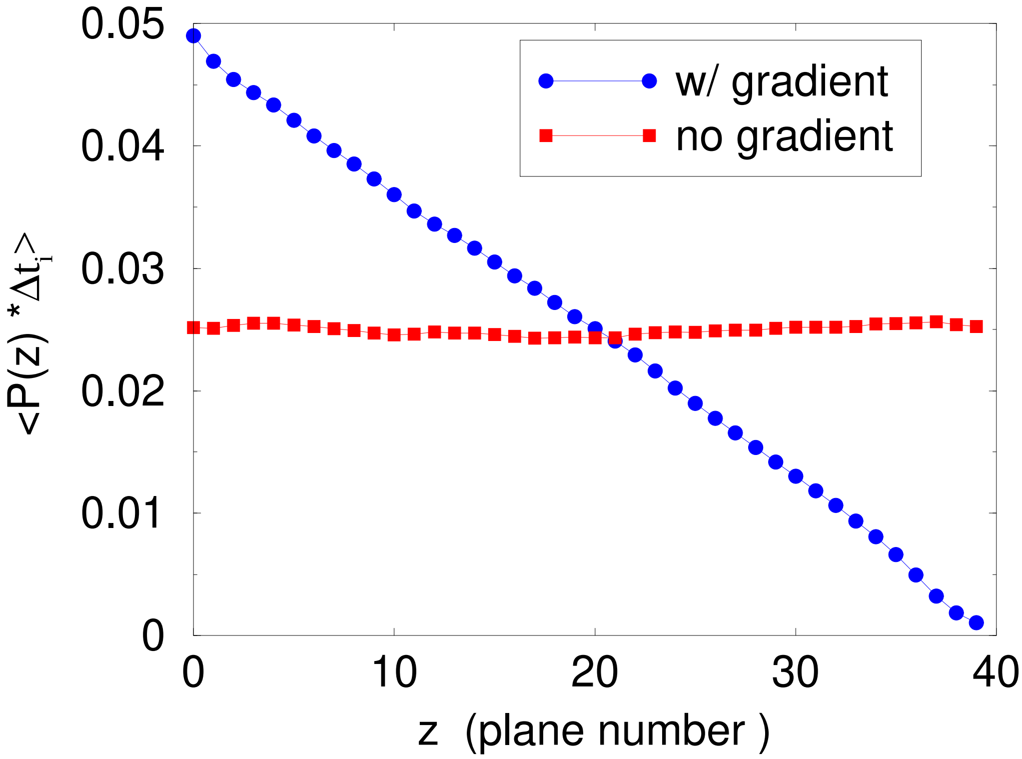

Figure 4.1: Time-averaged probability of finding a vacancy on one of the (001) planes, perpendicular on the gradient direction (labeled from 0 to 39) from KLMC simulations with and without a vacancy gradient present. The number of sites was 8×10^3; the bias parameter was $b = 2$.

gradient direction (we have four equidistant planes per unit cell) has a constant gradient, while there is no dopant gradient.

From Eq. 4.4 we see that γ can be found if we know the dopant flux and the dopant diffusivity, with a vacancy gradient present as shown in Fig. 4.1. The dopant flux is calculated from the dopant mean displacement. As was observed in lattice-gas models for binary alloys [24], the mean displacement is self-averaging, hence we monitored this quantity for sufficiently long times. This technique allowed us to obtain more accurate results than in our earlier work [29]. In Fig. 4.2, one can see the mean displacement versus time for As at different temperatures. While the

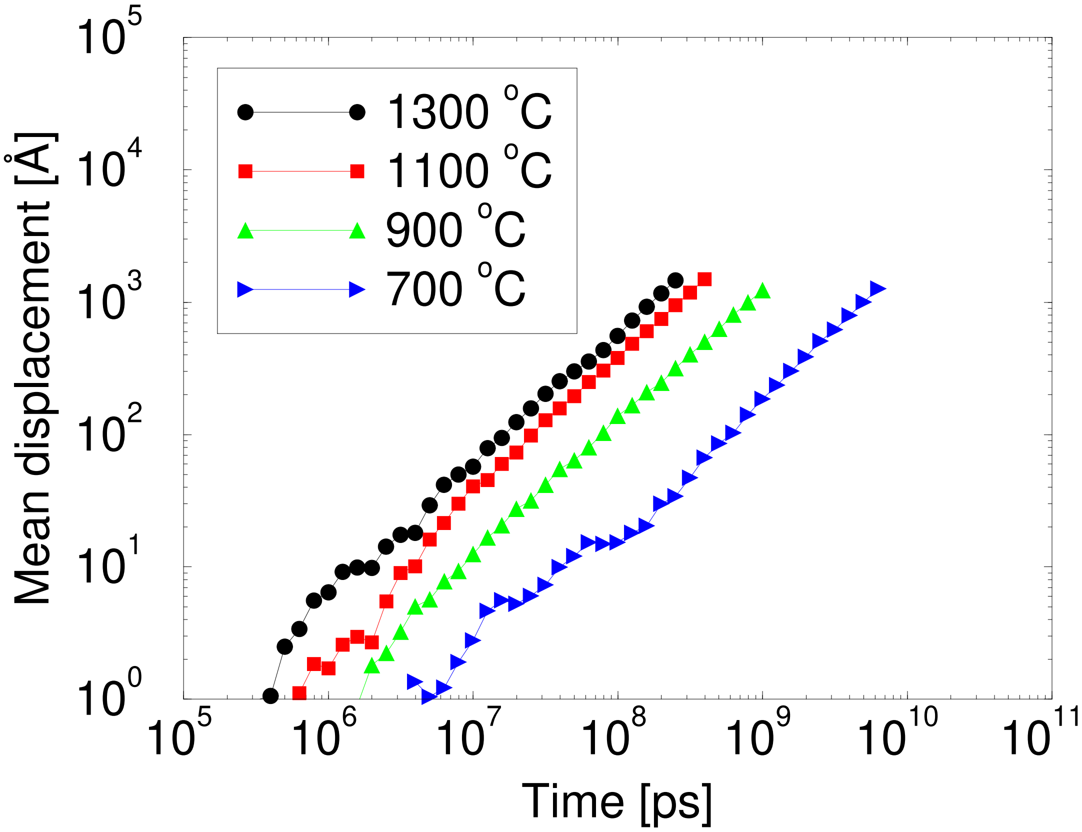

Figure 4.2: Mean displacement of As as function of time in a vacancy gradient for different temperatures. The number of sites was $8{\times}10^3$; the bias parameter was $b = 2$.

mean squared displacement of the dopant in a vacancy gradient could be used to find dopant diffusivity by subtracting the drift term, the diffusivity obtained in this way is noisy and a run with no vacancy gradient was preferred. Mean squared displacement for As at four temperatures is shown in Fig. 4.3.

Shorter times were used and many more simulations (a few hundreds) were performed to reduce statistical errors. Tests performed for As at 1300°C with cells of $6.4{\times}10^4$ sites found the same value for γ as with $8{\times}10^3$ sites, so the smaller system was used for the bulk of the simulations. For mean displacements larger than 50 Å, the standard deviation of the mean is smaller than the size of the symbols in Fig. 4.2

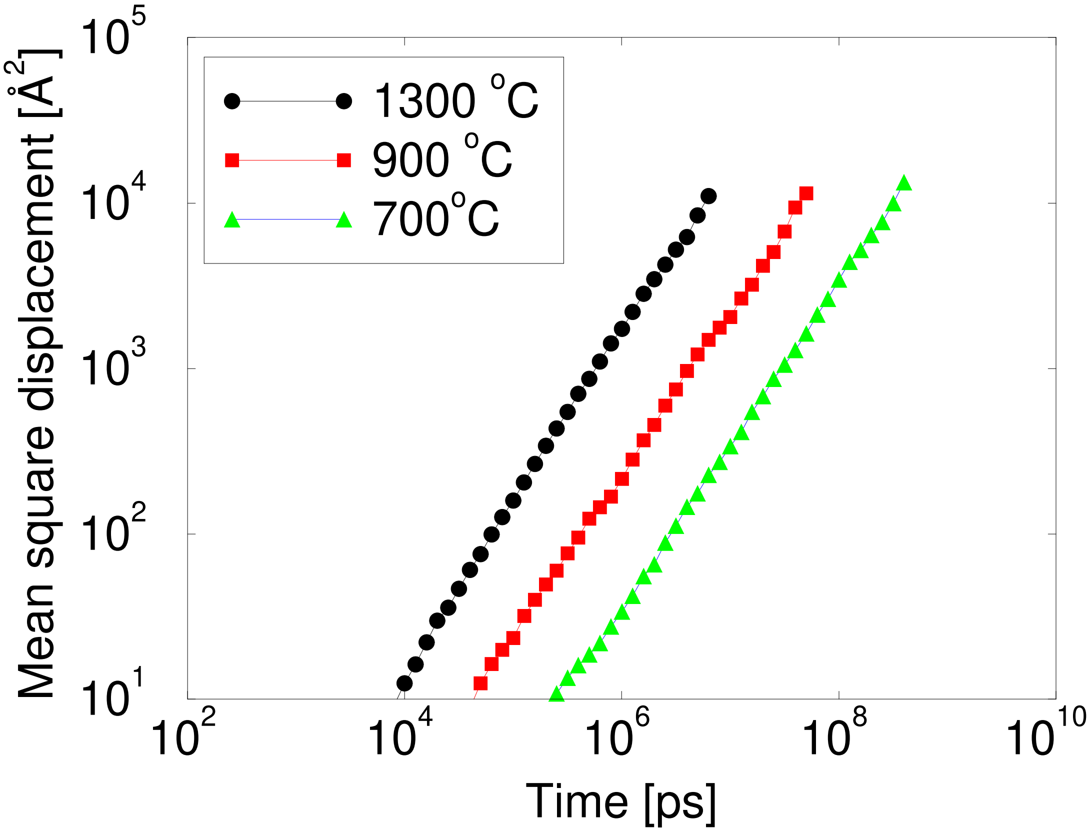

Figure 4.3: Mean squared displacement of As as function of time with no vacancy gradient for different temperatures. The number of sites was 8×10^3; the bias parameter $b = 0$.

and as such it is not shown.

We can look first at the diffusivity versus temperature as a test of the KLMC simulations and our understanding of the diffusion processes. For vacancy-mediated diffusion, a vacancy must separate to third-nearest neighbor distance and return along a different path in order for long-range diffusion to occur. Thus, for As, the pair diffusivity depends on the activation barrier between nearest neighbor binding and the second to third neighbor transition [$E_m + E_b^1 - (E_b^2 + E_b^3)/2 = 0.96$ eV]. For KLMC simulations with one vacancy and one dopant, the As-V pair diffusivity (proportional to $\exp(-0.96/k_BT)$) must be corrected by the probability that the

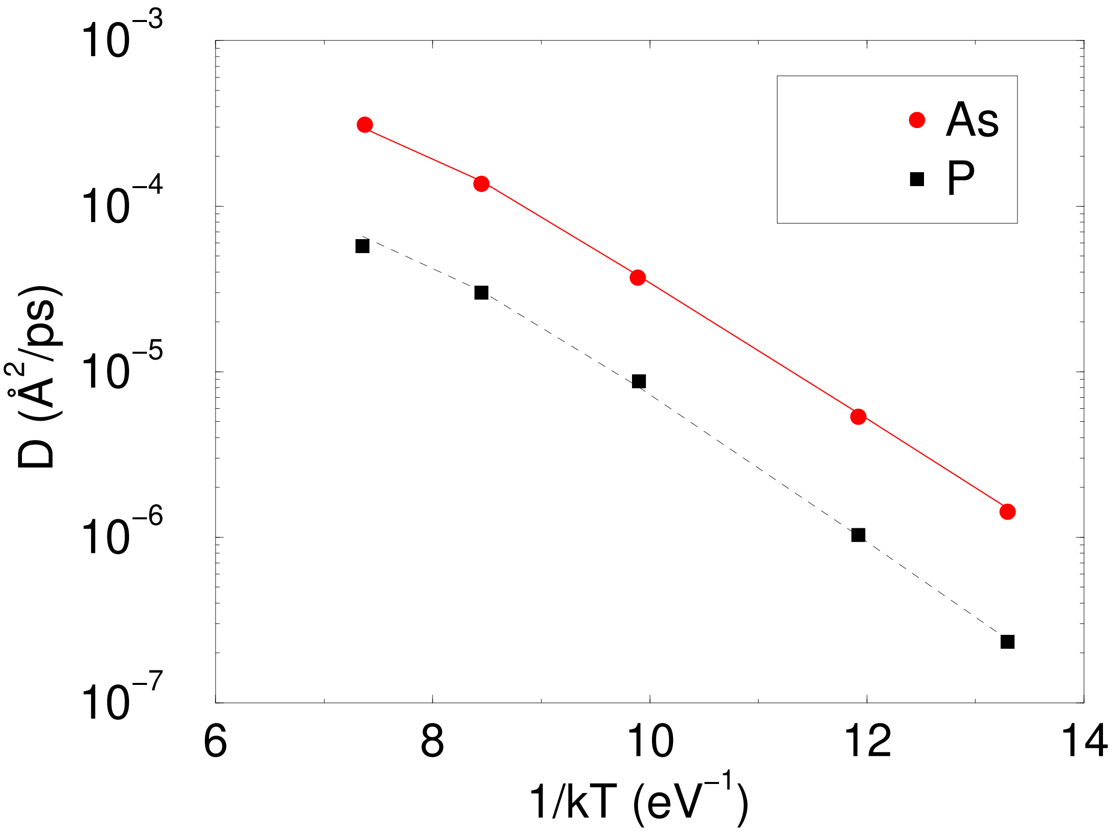

Figure 4.4: The As and P diffusion coefficients versus temperature from kinetic lattice Monte Carlo simulations with 8×10^3 sites, one dopant and one vacancy, and no vacancy gradient. Solid lines are predicted values.

dopant and vacancy are paired:

$$\frac{4\exp(1.17/\mathrm{k_B T})}{4\exp(1.17/\mathrm{k_B T}) + 8000} = \frac{1}{1 + 2000\exp(-1.17/k_B T)}, \tag{4.7}$$

where 4 is the number of first nearest neighbors, 8000 is the total number of sites in the simulation box, and 1.17 is the first nearest neighbor dopant-vacancy binding energy. This correction is more significant at high temperatures, leading to curvature on the Arrhenius diffusivity plot (as seen in Fig. 4.4).

Since the number of vacancies is fixed, the formation energy of a vacancy is not included. For P, pair diffusivity is limited by the large nearest neighbor exchange

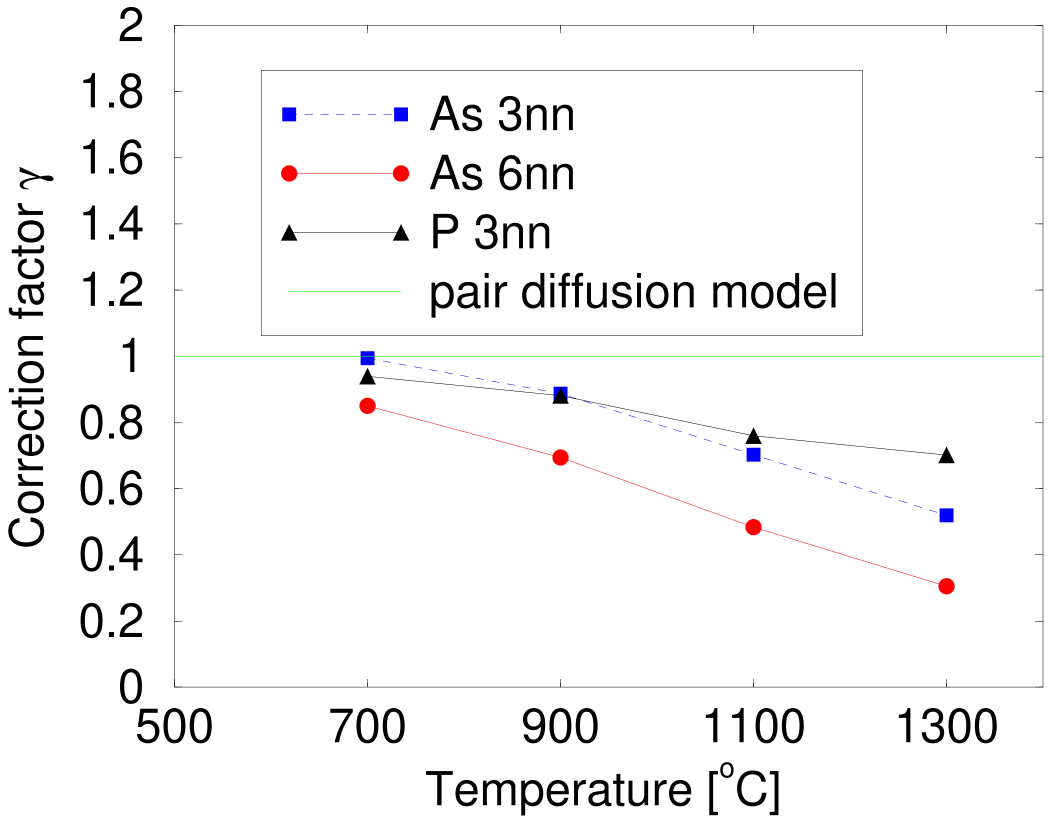

Figure 4.5: Correction factor γ from kinetic lattice Monte Carlo simulations for As and P as a function of temperature and range of interaction (3nn: third nearest neighbor interactions considered, 6nn: sixth nearest neighbor interactions considered). The number of sites was 8×10^3; the bias parameter was $b = 2$.

barrier (1.05 eV), which is well above that for the second to third neighbor transition (0.72 eV).

For As in a vacancy gradient, we find (Fig. 4.5) that the correction factor γ is positive, meaning that the As flux is in the same direction as the vacancy flux. At 700°C, γ is close to one, matching the prediction of the pair diffusion model. At higher temperatures, however, γ drops, with a value at 1300°C of about one third the value predicted by the pair diffusion model.

The basis for this behavior can be understood by considering the microscopic processes. Pair diffusion assumes that the pair is strongly bound and makes many hops before dissociating. As the temperature rises, the thermal fluctuations $k_B T$ become larger relative to the difference in activation energy between pair diffusion and dissociation, reducing the number of hops made before the pair breaks up. At the same time, the first dopant hop is likely to be in the direction *opposite* the vacancy flux as that is the direction from which the V is more likely to approach. As the number of hops for a pair drops, the bias induced by the first hop becomes more important dropping γ, which depending on the interaction potential can become negative [28], approaching the -2 value seen for tracer diffusion (in agreement with the statistical model of List *et al.* [21]).

The values of correction factor γ are smaller if interactions up to sixth nearest neighbor (current ab initio results are available only up to this range for As) are taken into account. This can be understood by noting that a longer-range interaction is associated with a larger effective capture cross-section, and thus conversely also an increased dissociation rate.

For P, the large exchange barrier leads to two significant changes relative to As. First, the large barrier reduces the number of hops made by the pair before breaking up, thus tending to reduce γ. Second, since exchange is inhibited, captured vacancies are likely to diffuse in the neighborhood of the dopant (separating to third neighbor distance and returning) before exchanging, greatly reducing the bias associated with the initial hop. The net result of these two compensating effects is a weaker temperature effect than for As. At lower T, γ is smaller for P than for As, while at higher temperatures P has a larger value of γ than for As (Fig. 4.5).

4.2 Capture Radius for Frenkel Pair Recombination

In continuum models [20], as well as Monte Carlo simulations which do not replicate the silicon lattice [32, 33], the annihilation between vacancies and interstitials is described by a capture radius which is not well characterized. Previous tight binding molecular dynamics calculations [16] showed that there is a long range interstitial-vacancy interaction extending up to the sixth-nearest neighbor distance. In order to quantify the interstitial-vacancy interaction more completely, molecular dynamics calculations were performed (by P. Fastenko [34]) using a recently developed environment dependent interatomic potential (EDIP) [35, 36, 37]. Those results are then used in KLMC simulations to determine the capture radius for Frenkel pair recombination and how it depends on the interaction range.

Constant temperature MD with an environment dependent interatomic potential (EDIP) [35, 36, 37] was used for the calculation of the interaction potential between interstitials and vacancies as a function of relative location. For each configuration, the atomic positions were relaxed at 0.1K to obtain the total energy of the system. Calculations confirm that the $\langle 110 \rangle$ split interstitial is the lowest energy configuration for a single self-interstitial with formation energy of $E_{\mathrm{I}}^{f} = 3.4$eV. The calculated vacancy formation energy is $E_{\mathrm{V}}^{f} = 3.2$eV. A 512 atom supercell was used. Test calculations with a supercell size of 1728 atoms give formation energies within 0.1 eV.

Initial conditions in KLMC method are obtained by having the vacancy and the Si self-interstitial randomly located on a 3D lattice, as in the case of finding the capture radius for I-V recombination as function of interaction range. Transition rates for vacancy and interstitial satisfy detailed balance and are postulated to be

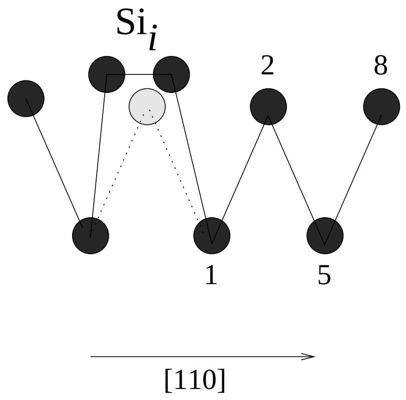

Figure 4.6: Numbers enumerate n-th nearest neighbor lattice sites for the vacancy relative to the split interstitial.

as in Eq. 4.5. The values of ν_m associated with interstitial and vacancy hops are chosen so that the diffusivities of isolated point defects match the TBMD [16] values of $D_v = 1.18 \times 10^{-4}\exp(-0.1/kT)$ cm^2/sec and $D_i = 0.158\exp(-1.37/kT)$ cm^2/sec.

I-V interactions energies versus distance are calculated via MD calculations as described above. As initial conditions, a split interstitial is placed at one site and an atom is removed from another site creating a vacancy. The system is then relaxed via MD and the energy and configuration saved. This process is repeated for different initial vacancy-interstitial displacements. We find that the vacancy-interstitial interaction potential depends strongly not only on distance, but also on direction (Fig. 4.7). Specifically, at short range the binding energy is much larger for vacancies located in the direction of buckling of the split interstitial ("up" in Fig. 4.6), with minimal binding even for close proximity in the opposite direction ("down"). The analysis shows that long range interactions are present, particularly along the $\langle 110 \rangle$ chain oriented in the direction of the split interstitial (0.6eV at fifth nearest neighbor distance).

In continuum [20] and off-lattice Monte Carlo [32, 33] models for dopant diffusion

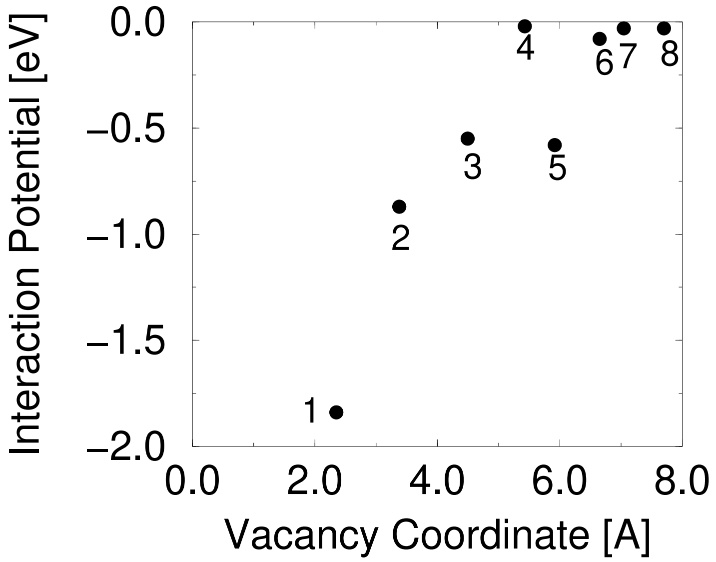

Figure 4.7: EDIP [35, 36, 37] potential has been used to calculate the interaction potential between an interstitial and a vacancy as a function of distance [34]. A long-range binding was found which depended strongly on the displacement direction relative to the orientation of the split interstitial. The distance (vacancy coordinate) is measured relative to the ideal lattice sites where interstitial and vacancy were introduced.

in silicon, the annihilation between a vacancy and a self-interstitial is described by a rate constant:

$$k_{I,V} = 4\pi a_{I,V}(D_I + D_V), \tag{4.8}$$

where the capture radius $a_{I,V}$ is often chosen arbitrarily. Since KLMC simulations explicitly include the silicon lattice structure, the Frenkel pair recombination rate $k_{I,V}$ and thus the capture radius can be calculated based on the I-V interaction potential as obtained from MD. Using initial random I and V displacements within a simulation box of volume Ω with periodic boundary conditions, the recombination

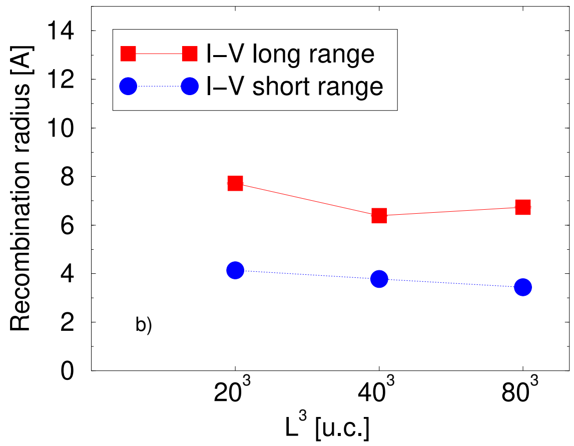

Figure 4.8: Capture radius for Frenkel pair recombination ($a_{I,V}$) with short (1NN) and long (6NN) range interstitial-vacancy binding as calculated with different system sizes expressed in number of unit cells [34].

rate is given by:

$$k_{I,V} = \frac{1}{\langle\tau\rangle\Omega}, \tag{4.9}$$

where $\langle\tau\rangle$ is the average recombination time. In Fig. 4.8, one can see that for short range interaction (first nearest neighbor binding which results in second nearest neighbor capture) the capture radius is 3.5 Å. The capture radius is 6.7 Å if long range interaction is taken into account (up to sixth nearest neighbor). With no I-V interaction (and thus only nearest-neighbor capture) the capture radius is 2.21Å. These calculations were performed at 900°C. It is found that the capture radius increases slightly as the temperature is reduced, as might be expected since at low T the capture probability increases for the weaker binding energies seen at larger distances.

In summary, molecular dynamics calculations show the existence of a long range interaction between vacancies and silicon self-interstitials which extends up to eighth nearest neighbor. This interaction is dependent on separation distance, but also on the direction of displacement of the vacancy with respect to the orientation of the split interstitial. This long-range interaction increases the rate of Frenkel pair recombination. Interstitial-vacancy recombination makes a big difference in ion implant annealing as will be discussed in Chapter 6.

Chapter 5

Anomalous Diffusion in Highly Doped Silicon

At very high concentrations, anomalous dopant diffusion behavior has been observed. Rapid thermal annealing (RTA) experiments by Larsen [38] made at 1050°C for 10 seconds indicate that below a threshold concentration ($\sim 2 \times 10^{20}$ cm^{-3}), the diffusivity of group IV and V impurities (As, Sb, Sn and Ge) increases linearly with dopant concentration, while above this concentration the diffusivity increases dramatically (see Fig. 5.1) with increasing donor concentration (proportional to C^n, n$\sim 3-6$). Earlier investigations [39] carried out over longer times (several hours) found that in the temperature range 1000–1100°C, the diffusivity of dopants (As) decreases rather than increases at very high concentration (see Fig. 5.2). Mathiot and Pfister [40, 41] proposed a percolation model. In this model, above a critical concentration dopant atom form a network and then they diffuse very fast within this network. Dunham and Wu [27, 42] proposed a Lattice Monte Carlo approach which provides a better description taking into account quantities like correlation factor, interaction range and random location of defects. It is usually assumed [3] that the

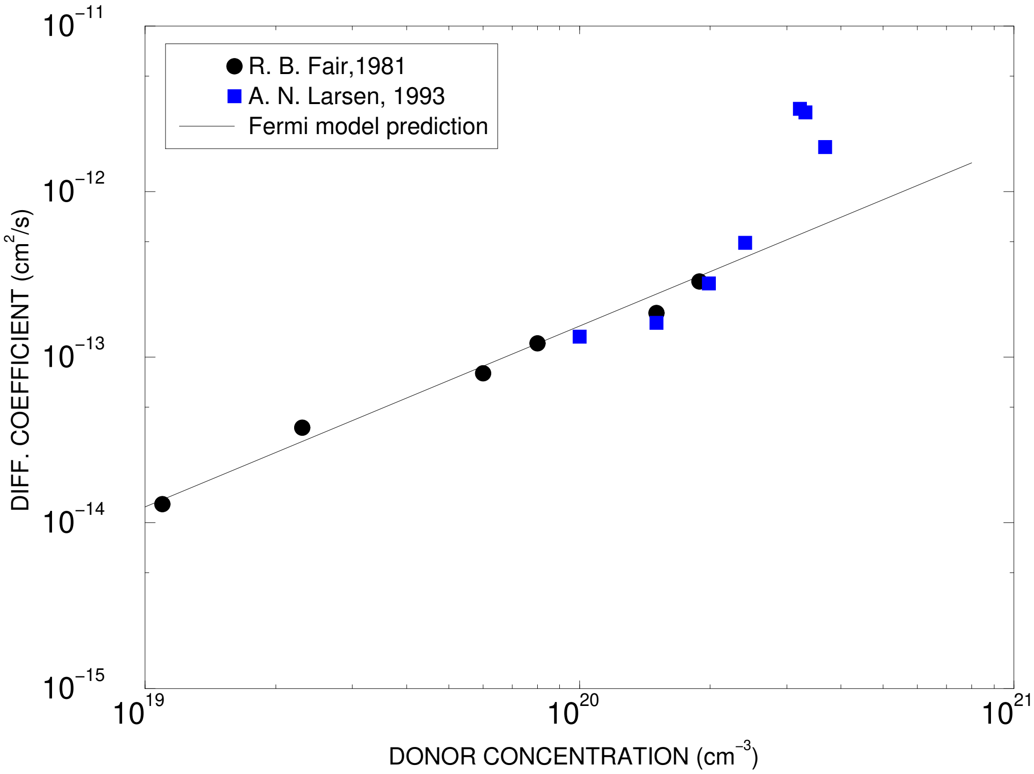

Figure 5.1: Diffusion coefficient as function of dopant concentration from isoconcentration experiments by Larsen *et al.* [38] and from Fair *et al.* [44].

potential energy of the vacancy is a superposition of a dopant-impurity attraction and a periodic potential experienced by the vacancy in the ideal crystal. Dunham and Wu made the additional assumption that the binding energy decreases linearly from the first to the third nearest neighbor and goes to zero on the fourth lattice site and obtained results that closely match Larsen. In contrast, List and Ryssel [43] found that diffusivity dropped with doping level using a similar interaction potential. They found an enhanced As diffusion with a nonattractive dopant vacancy interaction. However ab initio calculations [5, 6] find an attractive dopant vacancy interaction.

In this chapter, anomalous diffusion of As at high concentrations is studied using the KLMC method with dopant defect interaction from first principles calculations

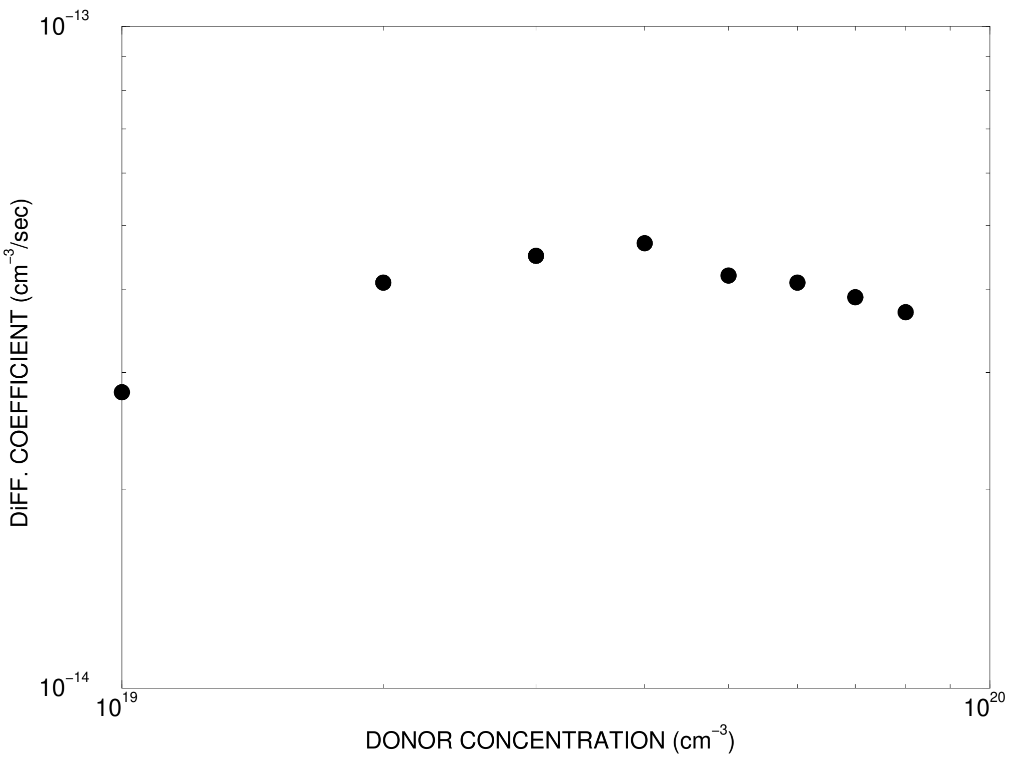

Figure 5.2: Diffusion coefficient as function of dopant concentration from experiments by Fair *et al.* [39] for indiffusion of arsenic at 1058° for 8h.

and interaction range up to sixth nearest neighbor distances.

5.1 Simulation Results

Impurity diffusion and aggregation depend on the underlying atomic-level processes. Recently it has become possible to use ab initio calculations based on density functional theory and the local density approximation (introduced in Chapter 3) to investigate these atomic-scale processes. As an example that will be applied in this work, the binding energies for dopants, vacancies and related clusters in silicon have been calculated as functions of the local configuration by several groups [5, 7, 46] (see Chapter 2). In contrast with simple pair diffusion models which provide the basis for most continuum modeling, these calculations show that relatively long-range interactions exist between dopants and vacancies (out to at least tenth nearest neighbor distances). The presence of long-range interactions opens the door for relatively complex interactions among multiple dopants with multiple vacancies, particularly at high doping levels. In order to explore how the nature of these dopant-vacancy interactions controls macroscopic diffusion and aggregation behavior, the Kinetic Lattice Monte Carlo method (introduced in Chapter 3) is applied.

In the KLMC simulations, periodic boundary conditions are used on a three-dimensional (3D) array of cubic cells, each with 8 lattice sites as in the silicon (or diamond) structure. Dopant-vacancy interactions are specified in terms of energy as a function of atomic configuration. Interactions energies are assumed to be additive. To initialize the system, dopants are placed randomly within the 3D structure according to the designated doping density. The vacancies are then placed with the probability of occupation depending on the binding energy for each site as calculated based on the dopants in the neighboring region:

$$p_V = \frac{p_V^0}{p_V^0 + (1 - p_V^0)\exp(\Delta E/kT)} \tag{5.1}$$

where p_V^0 is the probability of occupation for sites far from any dopant atom, k is Boltzmann's constant and T is the absolute temperature. The energy ΔE is assumed to be given by:

$$\Delta E = -\sum_{i=1}^{n} n_i \Delta E_i, \tag{5.2}$$

n_i being the number of dopants atoms as i^{th}-nearest neighbor and ΔE_i the corresponding dopant-vacancy binding energy. We consider values of n between 3 and 6 in this work, since as recognized by Hu [45], long range migration of a dopant via vacancy-mediated diffusion requires separation to the third-nearest neighbor (3NN) site with respect to a dopant, while the long-range migration of an As_2V complex requires dopant-vacancy separation to a 6NN distance. Values for the arsenic-vacancy binding energies are used from the ab initio calculations of Pankratov [5] (see Table 1, Chapter 2). The system evolves by considering the hopping of vacancies (actually the hopping of adjacent atoms onto the vacant site) with transition rates from Eq. (3.10). At each step, we update the hopping rates for vacancies, choose a hop based on the relative rates, and increment the time. In the end, the mean squared displacement is calculated to obtain the diffusivity.

Previous calculations [27, 28] using rough estimates of dopant-vacancy binding energies provided good agreement with the experimental observations of Larsen [38], predicting both the doping level at which the onset of enhanced diffusion occurs and as well as the dependence of diffusivity on increasing concentration. Using parameters from ab initio calculations in the framework of 3NN interactions, again a strong enhancement in diffusivity for high doping levels and short simulation times is found (see Fig. 5.3, noting that Fermi level effects have been normalized out). However, at longer simulation times it is found that the diffusivity enhancement decreases substantially (see Fig. 5.4), in agreement with experimental observations at longer times [39], the phenomenon being more pronounced at high doping levels. A comparison between diffusivity drop with time for different dopant concentrations is also shown in Fig. 5.5.

To understand this behavior the evolution in the number of As_xV complexes in the system is examined (see Figs. 5.6 and 5.7). The role of As_xV complexes in the overall diffusion process has been discussed recently by Ramamoorthy and Pantelides [46]. Based on their calculations, they proposed As_2V to be mobile and to have a significant role in the dopant diffusion. What KLMC simulations find is that

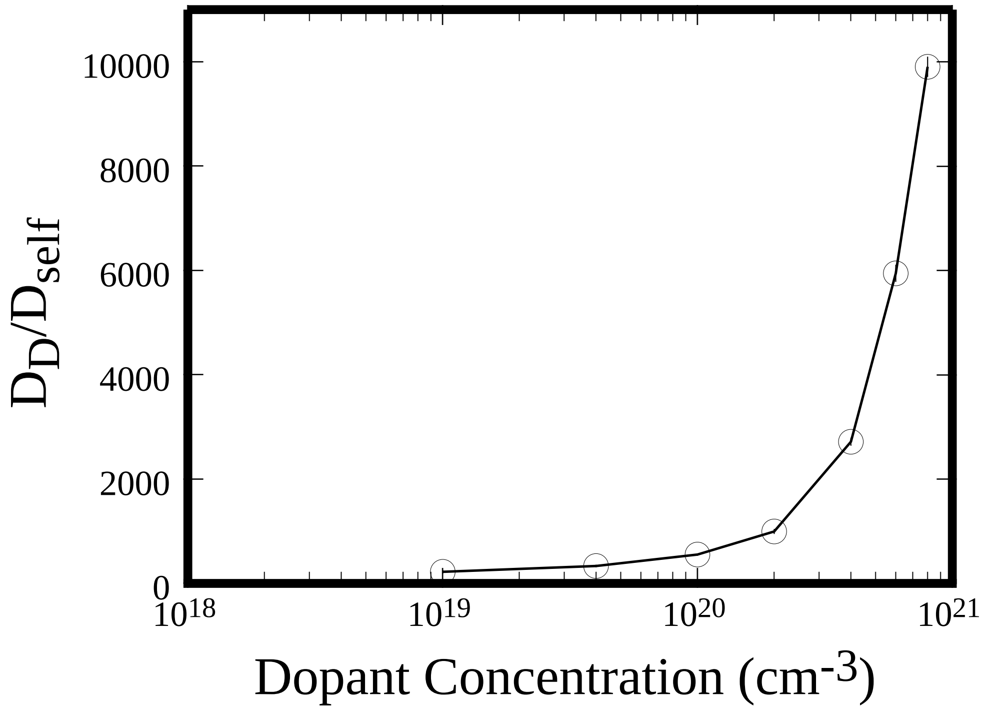

Figure 5.3: Normalized arsenic diffusivity versus doping density at 900°C from KLMC simulations using ab initio parameters [5, 6] after 10^4 t.u. 1 t.u. $= 1/\nu^0$ where ν^0 is the hopping frequency of a free vacancy. Note the strong increase above C$= 2 \times 10^{20}$cm^{-3}. The normalized diffusivity is obtained by dividing by the vacancy component of silicon self-diffusion ($D_V C_V^*$), thus removing the Fermi level dependence.

because of the strong dopant-vacancy binding, at high doping levels the number of As_2V complexes is higher than the number of AsV pairs and that their number grows with time, while the number of pairs decreases. As time progresses larger clusters such as As_3V and As_4V supplant the As_2V complexes. Since the larger complexes are much less mobile than the pairs, this is the source of the diffusivity reduction observed in our simulations.

To investigate further the role of As_2V complexes, the dopant-vacancy interaction is extended up to the sixth-nearest-neighbor (6NN) distance, since for long-range

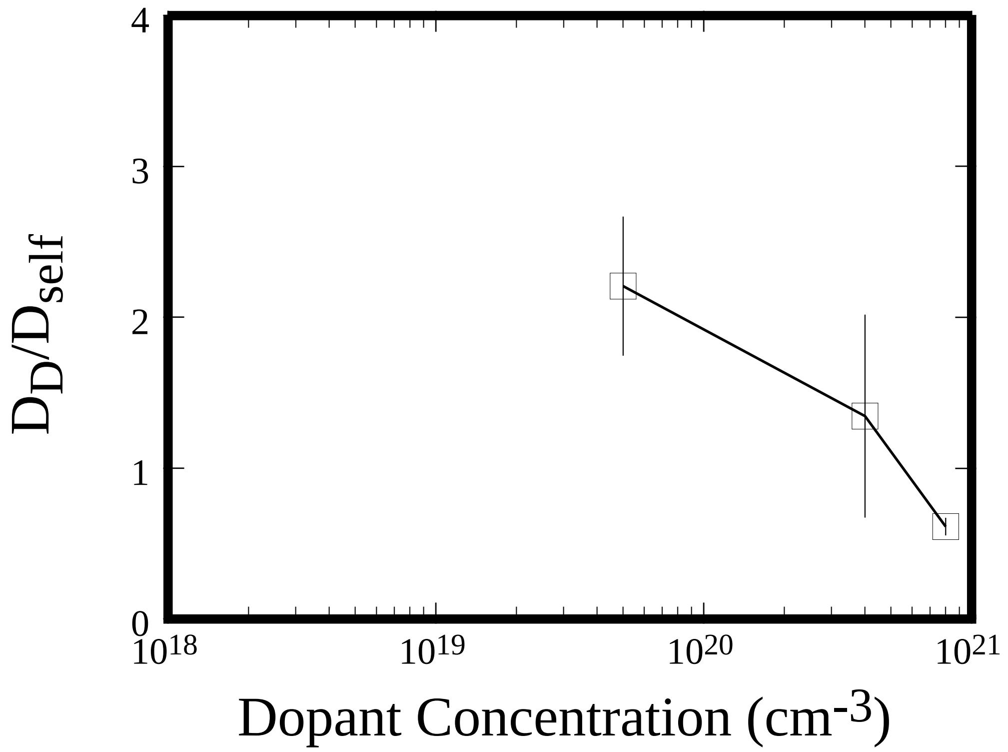

Figure 5.4: Normalized arsenic diffusivity versus doping density at 900°C from KLMC simulations using ab initio parameters [5, 6] after 10^9 t.u. . The diffusivity actually drops rather than increases as in Fig. 5.3 due to clustering.

diffusion of the As_2V it is necessary for the vacancy to move away until it is at distances of 3NN and 6NN from the two dopants, respectively. By examining the motion of isolated complexes (e.g., a one vacancy, two arsenic atom system), it is found that the diffusivity of As_2V complexes is about 50 times smaller than that of pairs at 900°C. However, as seen in Fig. 5.6 and Fig. 5.7, at high doping levels the number of As_2V complexes greatly exceeds that of pairs, so these complexes can have a significant role in diffusion. Also in Fig. 5.10 one can see how after a very long simulation time vacancies are trapped in As_xV clusters. In fact by combining the

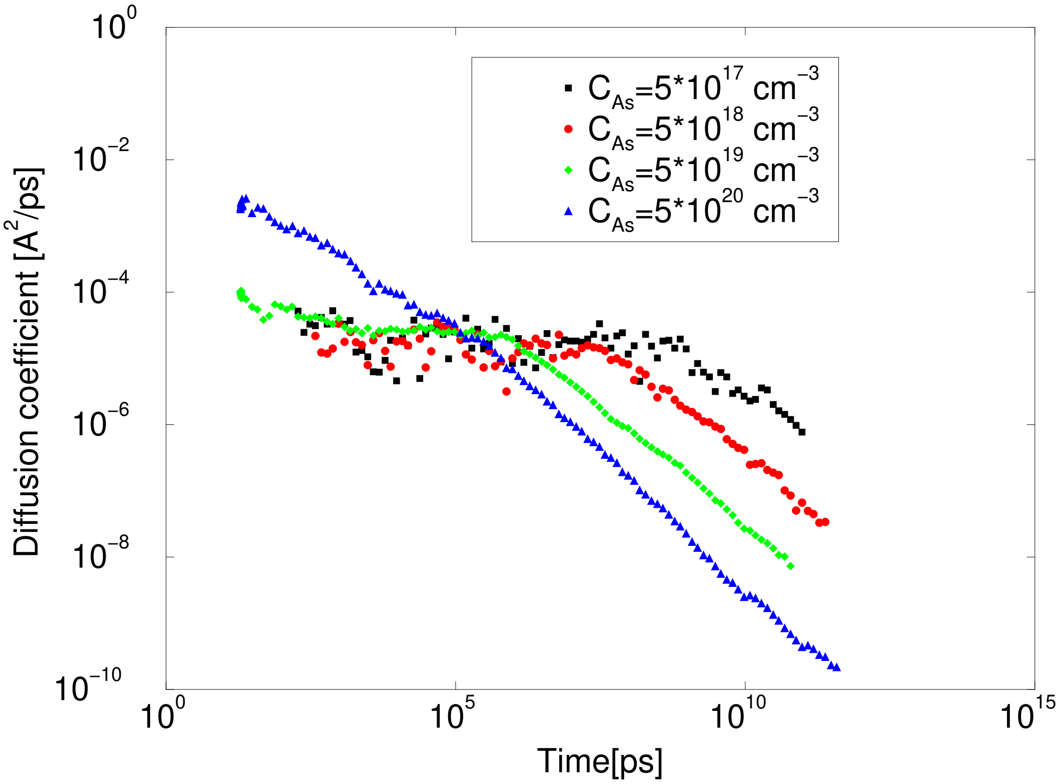

Figure 5.5: Arsenic diffusivity versus doping density at 900°C from KLMC simulations as function of time.

equilibrium concentrations of complexes with their diffusivity, it is found that for a concentration of 10^{20}cm^{-3} at 900°C, the contribution of As_2V to diffusion exceeds that of pairs (Fig. 5.8). However, a transition from diffusion dominated by pairs to domination by As_2V leads only to an increase of one in the order of the diffusivity increase with doping, in contrast to the much more abrupt increase observed both experimentally and in KLMC simulations. Thus, although mobile complexes may play a significant role at high concentrations, the rapid increase in diffusivity with doping at very high levels is due predominantly to collective effects involving the interactions of vacancies with multiple nearby dopant atoms.

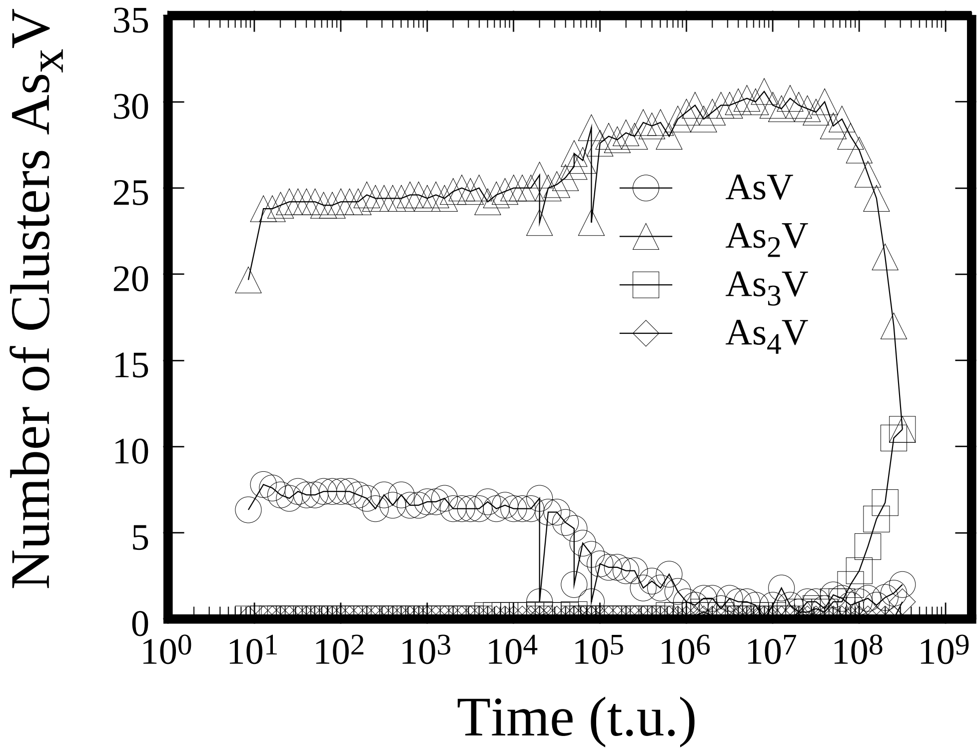

Figure 5.6: Number of As$_x$V clusters versus simulation time at 900°C for dopant density of 5×10^{19}cm^{-3}.

As the doping level in silicon changes, the position of the Fermi level changes also:

$$\frac{n}{n_i} = \exp\left(\frac{E_f - E_i}{kT}\right) \tag{5.3}$$

As a result, if vacancies are assumed to be single negatively charged then the concentration of vacancies is :

$$\frac{C_{V^-}}{C^i_{V^-}} = \exp\left(\frac{E_f - E_i}{kT}\right) \tag{5.4}$$

where $C^i_{V^-}$ is the concentration of negatively charged vacancies in an intrinsic ma-

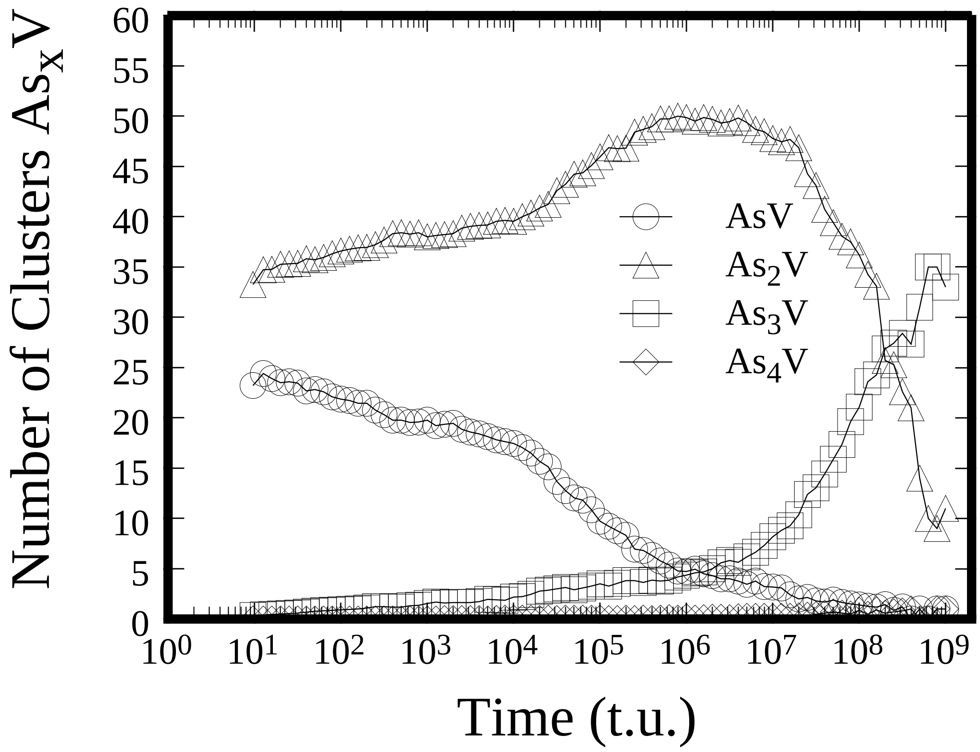

Figure 5.7: Number of As_xV clusters versus simulation time at 900°C for dopant density of $4\times10^{20}\mathrm{cm}^{-3}$.

terial. Fermi level effects are included in kinetic lattice Monte Carlo calculations by increasing vacancy concentrations as function of doping level according to the previous two equations. One can see in Fig. 5.9 the mean square displacement for three different dopant concentrations at 1050°C and $H_V^f = 3.65eV$, $S_V^f = 9k_B$ with a simulation box of 100^3 unit cells.

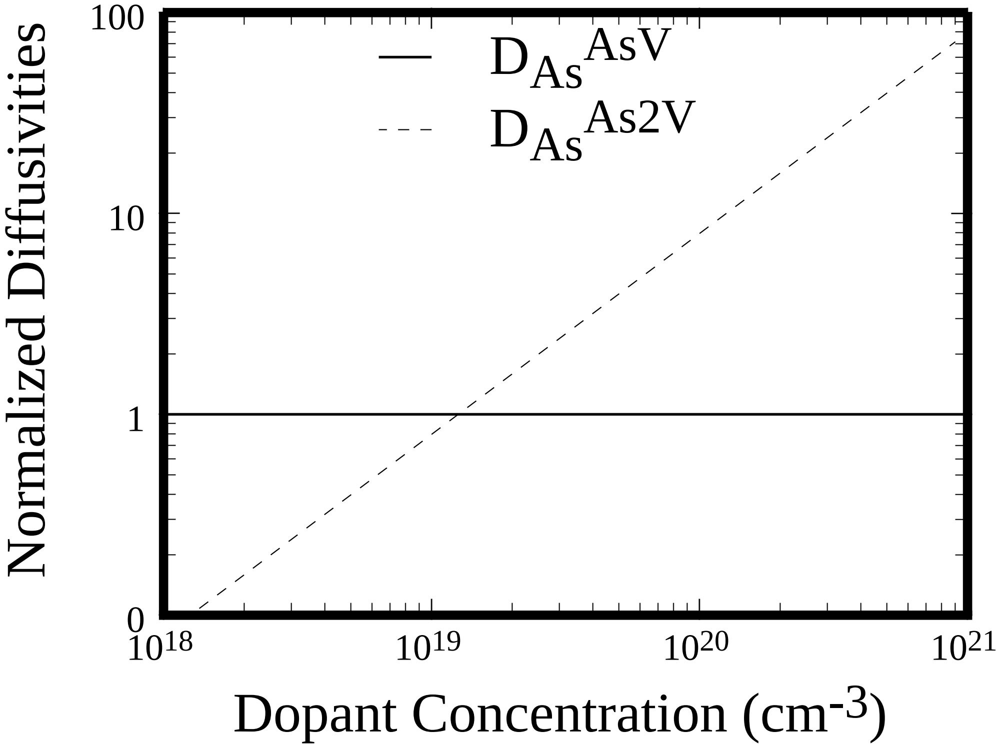

Figure 5.8: Relative diffusivities of arsenic due to AsV pairs and As_2V complexes versus doping level at 900°C with ab initio parameters [5, 6]. The contribution of As_2V to diffusion is predicted to dominate above $C_{As} = 2 \times 10^{19}\text{cm}^{-3}$.

5.2 Summary of High Concentration Effects

Dopant vacancy interactions from ab initio calculations have been used in Kinetic Lattice Monte Carlo simulations of vacancy mediated diffusion of As in silicon. A strong diffusivity enhancement for arsenic in heavily doped silicon has been found for short times, as observed experimentally [38, 44]. For longer times arsenic clustering takes place, again in agreement with experiment [39].

The role of mobile As_2V complexes was also explored, leading to the conclusion that these complexes are in fact mobile and can contribute significantly to diffusion,

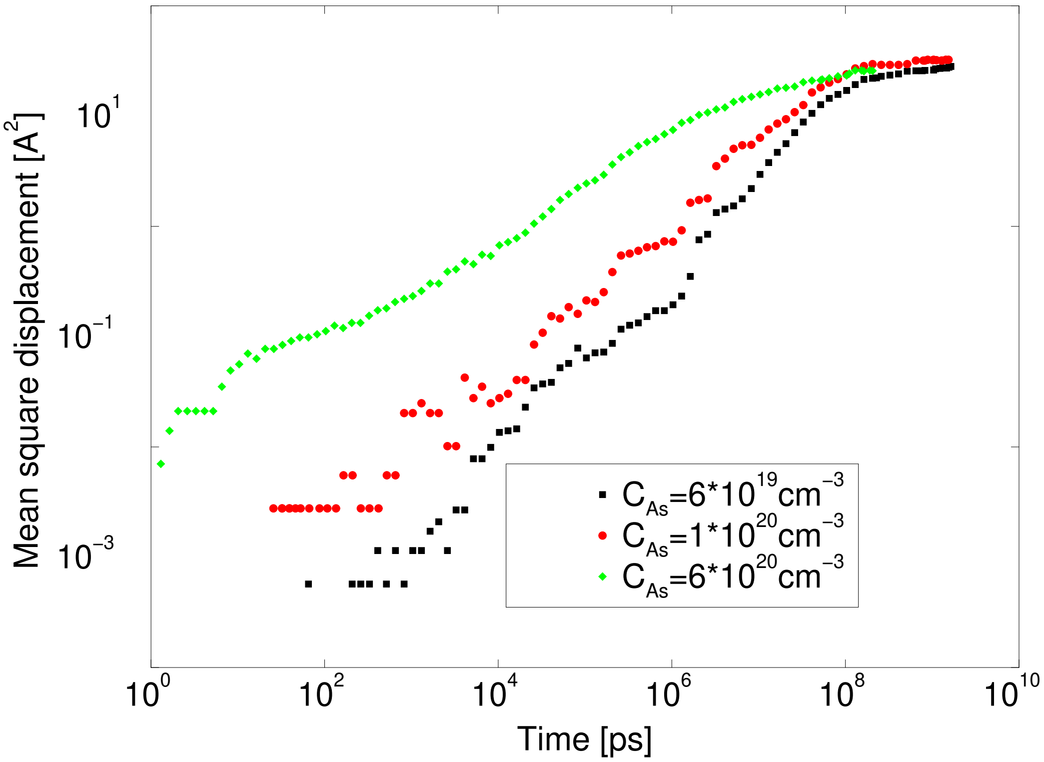

Figure 5.9: The mean square displacement as a function of time for three different dopant concentrations at 1050°C including Fermi level effects.

although their diffusivity is much smaller than the diffusivity of pairs, since they are present in higher numbers at high doping levels. However, the large enhancement in diffusivity at high doping levels is due primarily to collective effects involving the interactions of vacancies (even those in complexes) with several dopant atoms. List and Ryssel [43] found a reduction in diffusivity with doping level because they used relatively long simulation times. It should be noted that the As vacancy interaction assumed by List and Ryssel, Dunham and Wu, and this work is too strong, since the interaction energy was assumed to be additive. This is demonstrated by the fact that strong clustering is observed even at doping levels well below 10^{19} cm^{-3}. As As_xV clusters grow, the second, third and fourth As added actually have lower binding energy as noted by Ramamoorthy and Pantelides [46] and Berding *et al.* [47, 48].

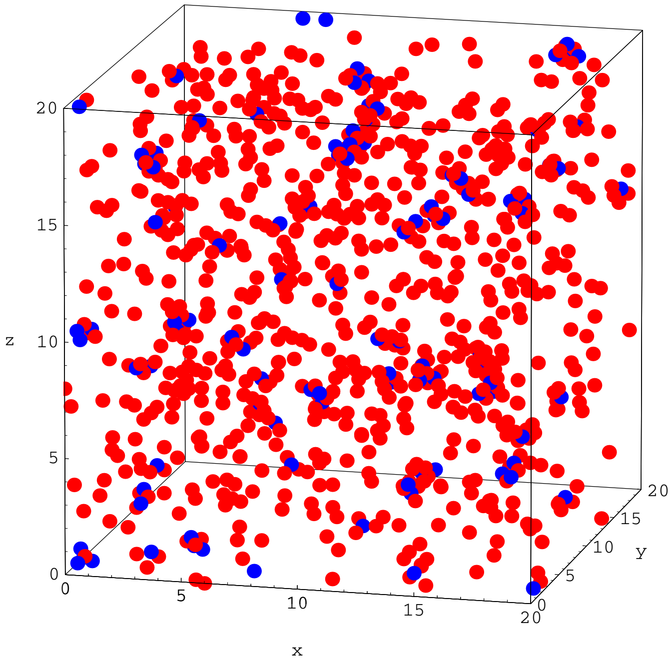

Figure 5.10: A 3D picture of dopants (grey atoms) and vacancies (black atoms) after a long simulation time when vacancies formed clusters with dopant atoms.

Also in Larsen *et al.* [38] experiments, a P background concentration ($\sim 4 \times 10^{20}$ cm^{-3}) up to the solubility limit was used, while in Fair *et al.* [39] experiment As was used to obtain the high doping concentrations, exceeding the concentration at which significant clustering occurs.

Chapter 6

Initial Stages of Ion Implant Annealing

Ion implantation is an efficient method for introducing dopants in silicon [49]. The implantation process produces considerable lattice damage due to the energetic collisions of ions with the lattice atoms. Understanding the damage evolution following ion implantation is crucial for accurately modeling transient enhanced diffusion (TED) [50, 51]. Present theories assume that TED is associated with the excess interstitials resulting from the implant damage, which aggregates into extended defects during annealing. The annealing process is often described through a +1 model [52] which assumes that after all Frenkel pairs generated during ion implantation recombine, the number of interstitials left equals the number of implanted ions.

Corrections to the +1 model in the form of "effective +N" models [33] have been proposed to account for differences in TED associated with changes in implant species and ion energies, as TED scales with the net excess interstitial concentration. It was found that heavy ions leave a larger number of interstitials after Frenkel pair recombination due to the greater separation between interstitial and vacancy profiles.

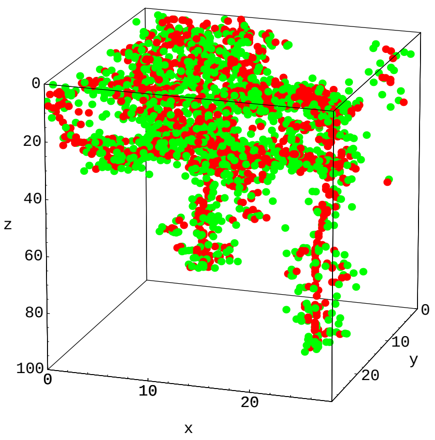

Figure 6.1: 3D distribution of point defects as obtained from an ion implant simulator. This distribution is called in text "initial spatial correlations." Dimensions of the simulation box are in unit cells (1 u.c.=5.43Å.)

Here the initial stages of damage anneal are studied by using the interstitial-vacancy interaction described in Chapter 2.

An important reason to use KLMC for simulation of the initial stages of implant annealing is that it is possible to account for the initial spatial correlations between the location of interstitials and vacancies following ion implantation (see Fig. 6.1). Continuum models specify only defect concentration with no correlation. Figure 6.2 shows a 3D distribution effectively equivalent to a continuum simulation generated with a depth distribution the same as from the ion implant simulator (UT-Marlowe) but randomly located in the plane perpendicular to the depth.

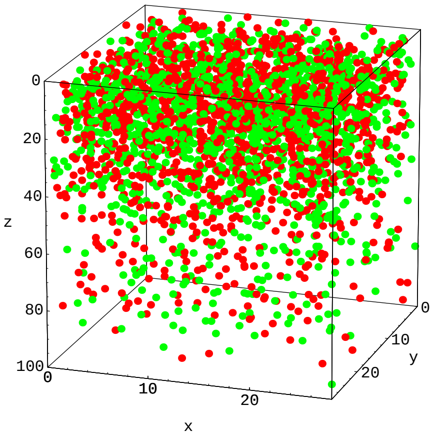

Figure 6.2: 3D distribution with random locations in the plane perpendicular to the depth for point defects. This distribution is labeled in text "no initial spatial correlations." Dimensions of the simulation box are in unit cells (1 u.c.=5.43Å).

6.1 Simulation of Damage Anneal

Initial conditions in KLMC method are obtained (a) by performing Monte Carlo implant simulations (UT-Marlowe [53]) that generate 3D distributions of dopants, vacancies and Si self-interstitials [54] (initial spatial correlations, Fig. 6.1) or (b) depth distribution of point defects is as in (a) but randomly located in the plane perpendicular to the depth (no initial spatial correlations, Fig. 6.2). The implanted ions are substituted by a Si self-interstitial. The values of ν_m associated with interstitial and vacancy hops are chosen so that the diffusivities of isolated point defects match the TBMD [16] values of $D_v = 1.18 \times 10^{-4}\exp(-0.1/kT)$ cm^2/sec and $D_i = 0.158\exp(-1.37/kT)$ cm^2/sec.

Pair interactions are considered in determining system energies. The binding energy for vacancy-vacancy and interstitial-interstitial interactions as well as for vacancy-interstitial interactions are described by the following expression:

$$E_X(i) = \sum_{Y,j} E_{XY}[N_Y(j)], \tag{6.1}$$

where $E_X(i)$ is the sum of binding energies for a point defect X (vacancy or interstitial) at site i with other point defects Y within the range of interaction. For example, $N_I(1)$ is the number of interstitials as first nearest neighbor to a given site and $E_{VI}(1)$ is the associated binding energy for a vacancy at that site. I-V interactions energies versus distance are calculated via MD calculations [34] Vacancy-vacancy and interstitial-interstitial interactions are chosen to match cluster binding energies from Jaraiz *et al.* [32]. The result (the number of interstitials left after vacancies recombine) was the same when cluster energies from Bongiorno *et al.* [55] were used, although the time required to eliminate all vacancies was longer. A look-up table was used for the simulation with cluster energies from Bongiorno *et al.* Only hops to first nearest neighbor sites are considered. The top surface is assumed to be a perfect sink and all the other surfaces are assumed to have reflection boundary conditions based on symmetry considerations.

The influence that the initial correlation of implant damage and the interstitial-vacancy interaction range has on the annealing behavior is studied through calculating the evolution in the net number of interstitials remaining (number of interstitials minus number of vacancies) as the Frenkel pairs generated during ion implantation recombine and diffuse to the surface. These excess interstitials are responsible for TED, which increases as the net interstitial excess increases. We define the +N number by the ratio of net interstitials to the implanted ions, which equals the interstitial excess in the +1 model. As shown in Figs. 6.3 and 6.4, the value of N increases

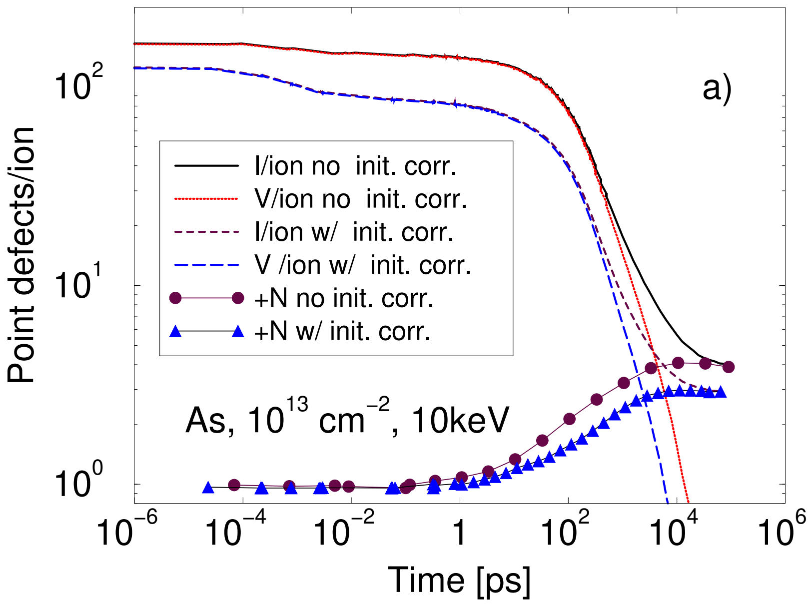

Figure 6.3: The number of point defects (vacancies and interstitials) per implanted ion and the +N number (net excess interstitials per implanted ion) as functions of time with and without initial correlations present for an As implant, 10 keV, 7° tilt, 30° rotation at 10^{13}cm^{-2} dose.

during recombination as the faster diffusing species (vacancies) diffuse to the surface. The +N factor after all the vacancies are gone is significantly reduced by the initial spatial correlations. This effect disappears at high doses.

Fig. 6.5 and Fig. 6.6 show how the +N factor depends on dose, implant energy, and modeling assumptions. The +N factor increases for lower doses, since the sparser damage increases the probability of vacancies making it to the surface. This increase is reduced when the initial defect correlations and long-range I-V interactions are included. The dependence on energy is more complicated. Although the effect is relatively weak, the +N factor appears to increase and then decrease with energy when the initial correlation is included, but only decrease with energy when the correlation is ignored. A possible explanation for this behavior is that N decreases at larger energies because the damage is located further from the surface and thus vacancies

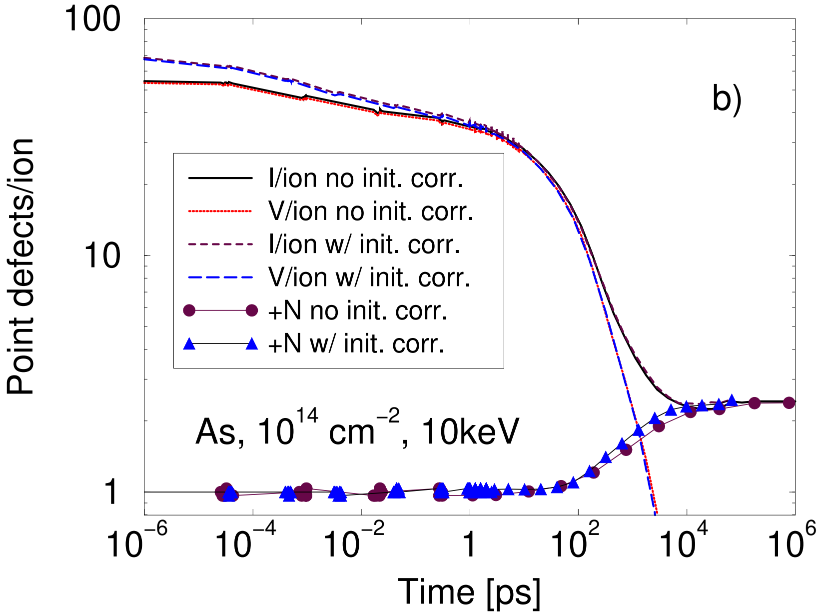

Figure 6.4: The number of point defects (vacancies and interstitials) per implanted ion and the +N number (net excess interstitials per implanted ion) as functions of time with and without initial correlations present for an As implant, 10 keV, 7° tilt, 30° rotation at 10^{14}cm^{-2} dose.

are less likely to make it to the surface before recombining. At lower energies, the separation between I and V increases with energy due to the increased momentum transfer. This effect, which is only included when the initial defect correlations are included, reduces the initial probability of Frenkel pair recombination. This effect becomes less significant at higher energies as electronic stopping becomes dominant.

For higher doses, the +N number appears to be almost independent of energy and modeling assumptions. This is due to the dense implant damage ensuring nearly complete Frenkel pair recombination. It may be noted that N does not reduce to 1, but instead to about 2 for arsenic implants. This is due to the separation between interstitial and vacancy distributions due to momentum transfer. When local Frenkel pair recombination is complete, a vacancy-rich region is left near the surface. These vacancies can diffuse readily to the surface, leaving greater than +1 excess

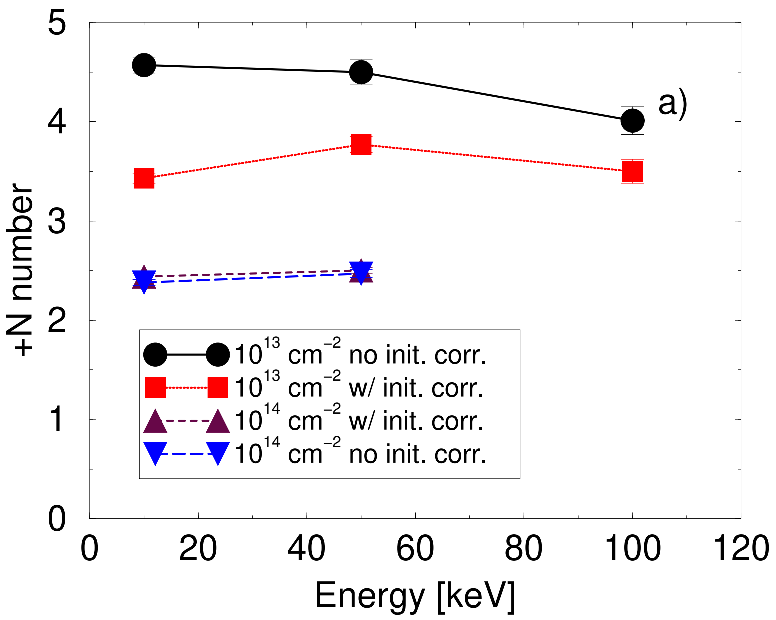

Figure 6.5: +N numbers after vacancies recombine for different doses and energies taking into account short range interaction between an interstitial and a vacancy. Cluster binding energies are from Jaraiz et al.[32] Interstitial-vacancy interactions from this work.

interstitials.

Atomistic techniques were used to explore the initial phases of ion implant annealing in order to predict the resulting effect on transient enhanced diffusion. Kinetic lattice Monte Carlo simulations were used to calculate corrections to the +1 model for effective damage distributions used in TED simulations as a function of dose, energy, and modeling assumptions. A "+N" factor was calculated which is proportional to the number of interstitials remaining after vacancies have recombined. This factor increases at lower doses since faster-diffusing vacancies can diffuse to the surface rather than recombining with interstitials. Using 3D damage distributions from MC implant simulations, it was found that the spatial correlations between vacancies and interstitials immediately following implantation is an important factor in determining the number of interstitials remaining after recombination. The long range I-V interaction determined from MD was also found to reduce the +N factor.

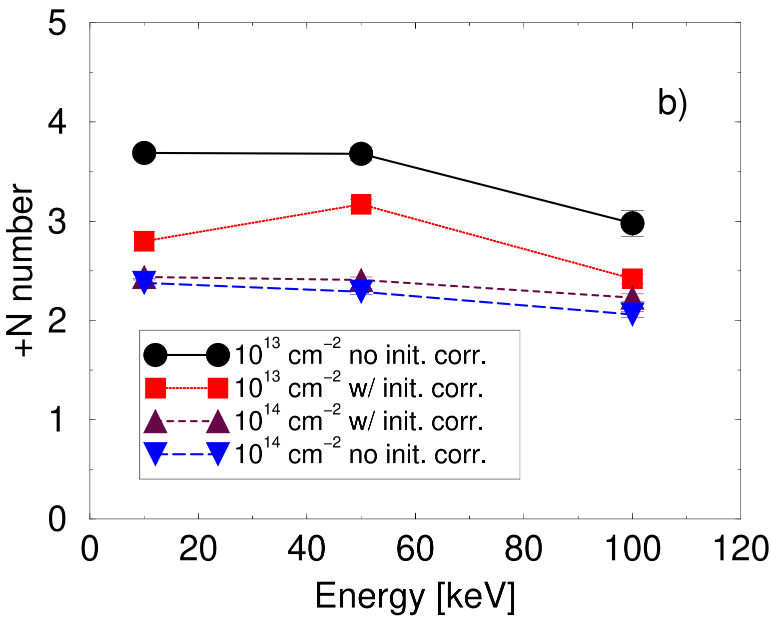

Figure 6.6: +N numbers after vacancies recombine for different doses and energies taking into account long range interaction between an interstitial and a vacancy. Cluster binding energies are from Jaraiz et al.[32] Interstitial-vacancy interactions from this work.

Chapter 7

3D Atomistic Simulations of Submicron Device Fabrication

It is predicted that by 2012 [57] MOS devices will have 50nm channel lengths and 20nm junction depths. A device with these dimensions and a dopant concentration of 10^{19}cm^{-3} has only 500 dopants in the channel region with the number of clusters and precipitates even smaller. Therefore for deep submicron devices, the atomic scale behavior will be important. Kinetic Lattice Monte Carlo [27, 29](KLMC) has emerged as an effective method for evolving a 3D system to times accessible by experiments. There are two reasons for this. On one hand, the fundamental time step in KLMC is related to hops (the time between $10^{-9} - 10^{-6}$ s) rather than the vibration period ($10^{-14} - 10^{-13}$ s) as in molecular dynamics simulations. On the other hand, the method considers only dopants and defects present in the system ($10^{10} - 10^{21}\text{cm}^{-3}$), which is much smaller than the atom density ($5 \times 10^{22}\text{cm}^{-3}$). In addition, as the devices become smaller continuum models become more complex, while KLMC computational requirements scale with L^3 and are inherently 3D.

7.1 Ion Implant Simulation

A Monte Carlo ion implant simulation (UT-Marlowe [53]) is performed to generate a 3D distribution of dopants, interstitials and vacancies. The patterned arsenic implant is a room-temperature implant, 5 keV, $4\times10^{14}\text{cm}^{-2}$ into (001) Si, 7° tilt, 30° rotation. The blanket boron implant is also a room-temperature implant 5keV, 10^{14}cm^{-2} into (001) Si, 7° tilt, 30° rotation.

7.2 KLMC simulation

Following the ion implantation it is assumed that in the regions where the concentration of interstitials is higher than $5\times10^{21}\text{cm}^{-3}$ the material is amorphous and recrystallizes defect free. As a result, interstitials and vacancies are removed from these regions. Also, since the anneal that is to be simulated is done at 900°C and KLMC calculations show a fast interstitial vacancy recombination at this temperature, nearest neighbor recombination for interstitials and vacancies is taken into account. The dopants and point defects are mapped to the nearest site on the silicon lattice. Then a box of $75\times75\times200$ unit cells, which represents a quadrant of an NMOS transistor, is chosen to be simulated using KLMC. The top surface, through which the implant has been made, is assumed to be a perfect sink for defects and all the other surfaces have reflecting boundary conditions. The mobile species considered in KLMC are vacancies, interstitials and dopant interstitials. Migration and binding energies used in simulations are presented in Table 1. For interstitial arsenic, ab initio results are not available, so an arsenic interstitial interaction similar to boron is assumed but with smaller binding energy for the As_s-I pair and no binding for the As_i-As_s pair. In KLMC the transitions rates are calculated according to Eq. (3.10).

The 3D picture of the 50nm NMOS quadrant with the locations of dopants is presented in Fig. 7.1, shown immediately after the ion implantation, (time=0), and after the KLMC simulated annealing at 900°C for time=10ms and time=0.1s. In Fig. 7.2 is shown the total number of point defects and interstitial dopants as functions of time. Between 1 ps and 1 ns, vacancies and interstitials are present in large numbers, the dominant processes being vacancy-silicon exchanges, interstitial hops and interstitial vacancy recombination. Dopants go from interstitial to substitutional state, either due to dissociation or interaction with vacancies. Looking at the number of boron clusters in Fig. 7.3 one can see that boron is mostly in the form of isolated boron interstitial pairs.

Next a time interval (1 ns to 1μs) is found where most of the dopants are in the substitutional state. After 1μs, vacancies exist mostly in the form of vacancy-arsenic clusters. In Fig. 7.4, a boron implant identical with the one used for initializing the MOS device is shown, but no arsenic. Here it is seen that vacancies disappear sooner. From 1μs one can also see that the boron starts pairing with interstitials. Initially one starts with isolated boron interstitials, but as boron interstitials migrate, they pair with substitutional boron. The number of B_i B_s complexes reaches a maximum at 0.1 ms when there is also a peak in the total number of boron interstitials in Fig. 7.2.

Table 7.1: Simulation parameters. Binding energies up to first nearest neighbor only.

binding energies	migration energies	exchange, kick-in and kick out barriers
$E(As\text{-}V)$=1.18 eV [5]	E_m^V=0.3 eV [58]	$E_{exch}(As\text{-}V)$=0.66 eV [5]
$E(As_s\text{-}I)$=0.6 eV	E_m^I=0.9 eV [11]	$E_{exch}(B\text{-}V)$=2.5 eV [6]
$E(As_i\text{-}As_s)$=0.0 eV	$E_m^{B_i}$=0.3 eV [11]	$E_{kick-out}(B)$=1.0 eV [11]
$E(B\text{-}V)$=0.17 eV [6]	$E_m^{As_i}$=0.3 eV	$E_{kick-in}(B)$=0.6 eV [11]
$E(B_s\text{-}I)$=1.0 eV [11]		
$E(B_i\text{-}B_s)$=1.8 eV [11]		

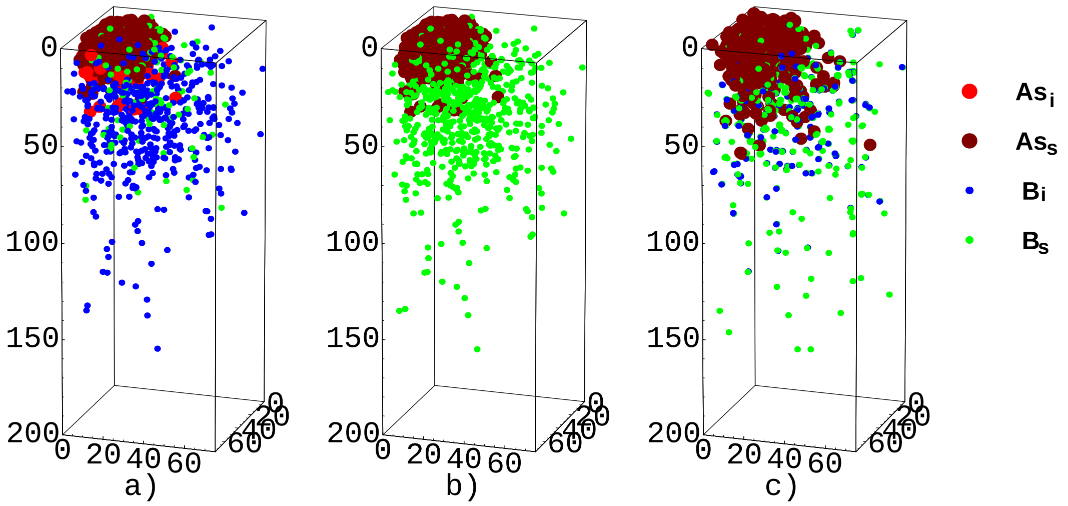

Figure 7.1: A quadrant (75×75×200 unit cells) of a 50nm nMOS transistor where dopants, arsenic and boron, in substitutional or interstitial state are shown, after ion implant simulation at (a) time=0 . Also shown is the evolution of this system during an anneal at 900°C at (b) time=10μs and (c) time=0.1 s.

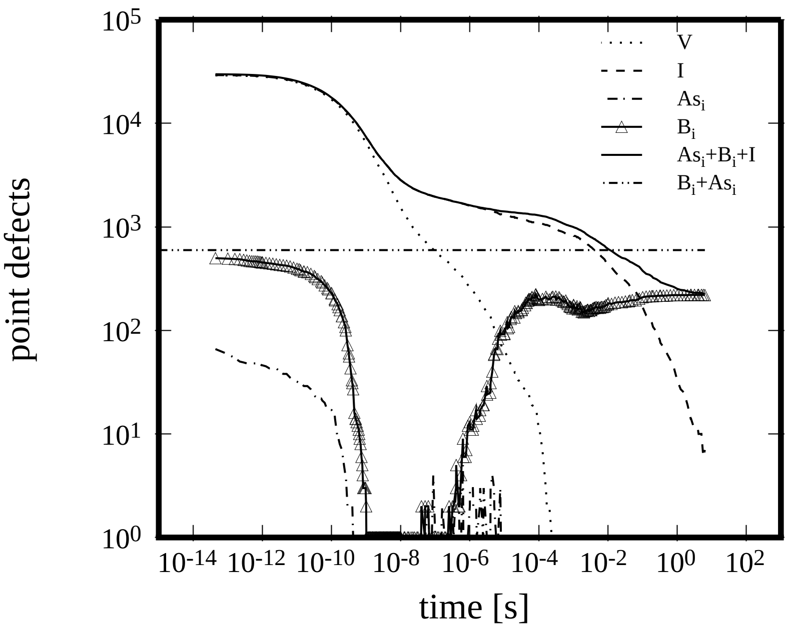

Figure 7.2: The number of vacancies, interstitials, dopant interstitials as a function of time. The horizontal line represents the total number of dopant interstitials at the beginning of the KLMC simulation.

As the interstitials reach the surface where they are annihilated, there is not enough interstitials in the system for the number of pairs to keep growing. Therefore they find more stable configurations in the form of larger clusters: B_3I (a boron interstitial with two substitutional boron as first nearest neighbor(1NN)), B_4I (one B_i and three Bs as 1NN) and B_5I one B_i and four Bs as 1NN). Given the energetics used here, these last clusters do not dissociate over the time that is simulated. It is expected that the large boron clusters grow and that small ones disappear freeing some interstitials in the process the same way the numbers of boron interstitial boron substitutional pairs decrease in favor of bigger clusters. It is found that the behavior of boron clusters is very much dependent on the binding energy of the boron interstitial-boron substitutional pair. A simulation with only 1 eV for this energy

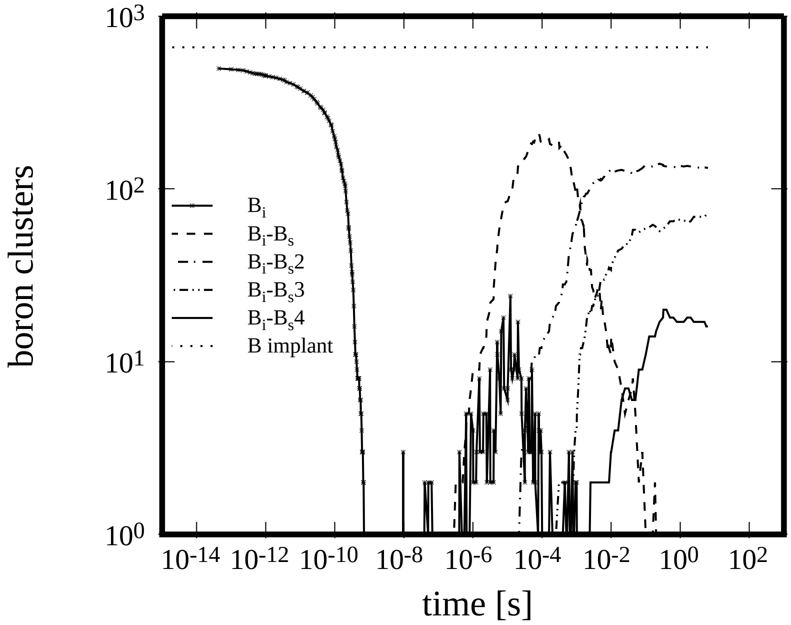

Figure 7.3: The number of boron interstitial clusters as a function of time. The horizontal line is the number of boron atoms implanted.

produces far fewer boron clusters. After 10s one can see that the number of total interstitials becomes smaller than the initial number of interstitial dopants due to the annihilation at the top surface.

7.3 Summary

We have shown that it is possible to simulate the fabrication of a 50nm MOS transistor with dopants and point defects distributions from an ion implant simulator and subsequent dopant diffusion performed with kinetic lattice Monte Carlo. A time interval in which dopants are mostly substitutional is found. The presence of arsenic makes vacancies last longer in the system due to arsenic vacancy clusters. Further

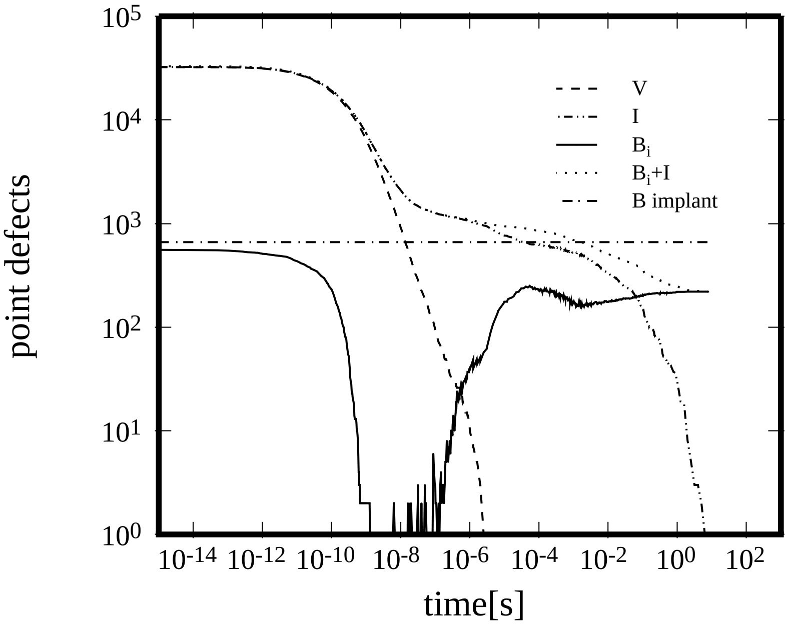

Figure 7.4: Number of vacancies, interstitials and boron interstitials as a function of time for the annealing of a boron implant, 5keV, $10^{14}\mathrm{cm}^{-2}$, 7° tilt, 30° rotation. The horizontal line is the number of boron ions implanted.

work will have to produce faster algorithms, since present simulations take about 50 hours as serial jobs on an R10000 processor. The dependence of energy on cluster size, and its influence on the overall system needs also further investigation, since the behavior of these clusters is very sensitive to the energies involved.

Chapter 8

Dopant - Defect Interaction

8.1 Boron - Interstitial Interaction

As was shown in Chapter 2, dopant impurities like boron diffuse via an interstitial mechanism. The impurity is converted for short time intervals into a fast migrating intermediate species, dopant interstitial B_i. The relevant reactions for diffusion via B_i are [59]:

$$I + B_s \rightleftharpoons B_i \tag{8.1}$$

$$V + B_i \rightleftharpoons B_s \tag{8.2}$$

$$I + V \rightleftharpoons 0 \tag{8.3}$$

Eq. (8.3) plays an important role by modifying the concentrations of interstitials and vacancies available for reactions (8.1) and (8.2).

The intermittent diffusion is more complicated than Fickian diffusion. Diffusion experiments [60] with nanometer scale boron doping profiles in silicon find that boron diffuses via an intermediate species. The resultant diffusion profile of an initial δ-function impurity distribution has exponential tails. The decay constant of the tail provides the mean projected path length λ, which has an anomalous temperature dependence (increases as the temperature decreases):

$$\lambda = \lambda_0 \exp(+E_\lambda/kT) \tag{8.4}$$

where λ_0 is the mean projected distance. Previous calculations [61] showed that reaction (8.1) is exothermic (1.0eV). This equation implies that as the temperature decreases the dopant migrates for longer distances.

In this work, the boron interstitial interaction is studied using the ab-initio method discussed in Chapter 3. Besides the use of density functional theory(DFT) and local density approximation (LDA), efficient plane-wave ultrasoft pseudopotential and a 4^3 Monkhorst-Pack k-point sampling are used. The code VASP [62] was used for these calculations. Also a 64 atom supercell is used throughout these calculations. The formation energy of the self-interstitial is defined as:

$$E_f(Si_i) = E(Si_{65}) - \frac{65}{64}E(Si_{64}), \tag{8.5}$$

where $E(Si_{65})$ is the total energy for a 65-atom supercell containing a Si self-interstitial and $E(Si_{64})$ is the total energy for a 64 atom supercell of pure bulk silicon.
The formation energy for the boron substitutional silicon self-interstitial pair is defined as:

$$E_f(B_s - Si_i) = E(Si_{64}B) - E(Si_{63}B) - \frac{1}{64}E(Si_{64}) \tag{8.6}$$

Si_i assisted boron diffusion starts from a bound pair of boron and Si_i. The lowest energy is found for a pair with boron substitutional and Si_i tetrahedral (see Fig. 8.1 upper left). The binding energy of this pair is 0.9 eV with respect to the most stable dissociation products Si_i^{T+} and B_s^-. A 0.7 eV barrier is found for kicking out boron from a substitutional position to a hexagonal site (see Fig. 8.1 upper right), which is significantly lower than the 1.1 eV barrier found previously [11]. Thus instead of following a hexagonal - tetrahedral path as found by Zhu *et al.* [11], boron kicks in immediately as boron substitutional. The energetics for the neutral systems is shown in Fig. 8.2. The activation energy for the diffusion mechanism described above is given by:

$$Q(B_s) = E_f(B - Si_i) + E_m(B_s) \tag{8.7}$$

and is found to be 3.0 eV which is the lower bound of the experimental range. This mechanism is also able to explain the anomalous increase in diffusion length with decreasing temperature the same way the kick-out mechanism does. As the temperature decreases the boron substitutional Si self interstitial pair is less likely to dissociate leading to an increase in the diffusion length. The activation energy for the mean projected path is found to be 0.65 eV, and explains the anomalous temperature behavior observed in experiment (increases with decreasing temperature), due to the fact that at lower temperatures boron interstitial makes more hops before the boron complex dissociates, thus increasing the mean projected path.

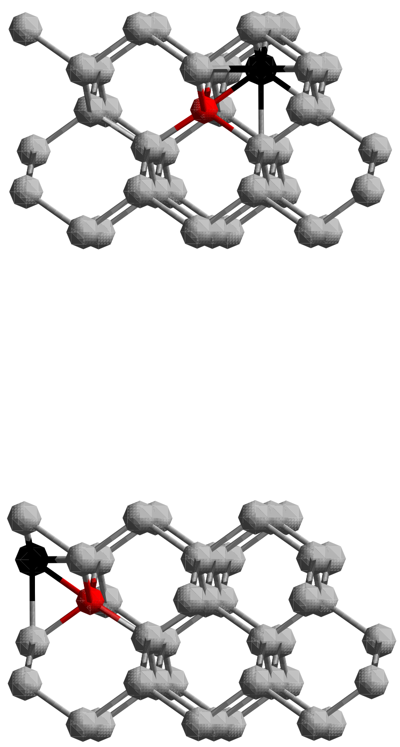

Figure 8.1: Boron diffusion in Si following a substitutional - hexagonal - substitutional path. In the upper left figure one starts with a boron substitutional Si self interstitial pair in a tetrahedral position. In the upper right figure boron is kicked-out into a hexagonal position becoming interstitial. In the lower left figure boron becomes substitutional again and in the lower right figure boron is kicked-out into another hexagonal position. The migration process ends when the pair dissociates.

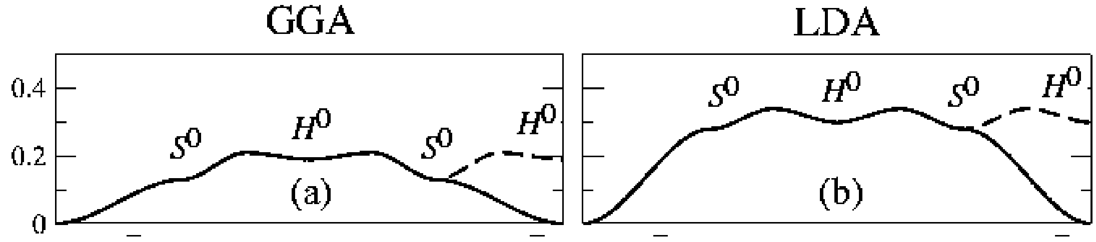

Figure 8.2: The nudged elastic band total energy (eV) for a neutral system relative to the energy of the initial system of $B_s - Si_i$ complexes as a function of the hyperdistance of the system from the initial configuration (a) within the GGA approximation, (b) within LDA approximation. See Windl *et al.* [9, 10] for complete details.

Chapter 9

Conclusions

In this research, the kinetic lattice Monte Carlo method was used to study dopant diffusion in silicon. A computer program (LAMOCA) was written to investigate diffusion with dopant defect interactions from recent ab initio calculations and diffusivities of vacancies and interstitials from molecular dynamics calculations. A model based on a lattice occupied by different particles (vacancies, interstitials, dopants, silicon atoms) with medium range interactions (up to tenth nearest neighbor) was employed with different boundary conditions. Transition rates were based on the change in the system energy and satisfy detailed balance.

Kinetic lattice Monte Carlo calculations of dopant diffusion in a vacancy gradient revealed that for As the dopant flux driven by a vacancy gradient has the same direction as the vacancy flux with a magnitude that approaches that of ideal pair diffusion at low temperatures (700°C) and drops with increasing temperature. The dopant flux decreases further below predictions of pair diffusion model if long range interactions are taken into account. In case of phosphorous, due to a large exchange barrier which becomes the rate limiting step for pair diffusion, a similar behavior is found but with a weaker temperature dependence, leading to dopant fluxes which are smaller at low temperatures, but larger at high temperatures. A correction factor which accounts for the smaller flux in a vacancy gradient has been calculated for applying corrections to continuum models.

Using the vacancy interstitial potential from molecular dynamics calculations, the capture radius for Frenkel pair recombination was found to be dependent on the interaction range. At short range interaction (first nearest neighbor) it has the value of 3.75 Å. Including full long range interaction (eighth nearest neighbor) it has the value of 6.5 Å. The capture radius was also found to increase slightly with decreasing temperature. The calculated capture radius can be used directly in continuum models where previously this quantity was assumed arbitrarily.

KLMC simulations show a large enhancement in diffusivity at high doping levels due primarily to collective effects involving the interactions of vacancies with several dopant atoms and to a much higher concentration of vacancies at those concentration levels. Dopant diffusion is found to decrease with time due to clustering. The dopant vacancy attraction potential is the source for clustering. The impact on diffusion of different As_xV complexes has been studied. Based on ab initio calculations, it was found that complexes like As_2V are mobile and may contribute significantly to diffusion.

The initial phases of ion implant annealing were explored in order to predict the resulting effect on transient enhanced diffusion (TED). A factor +N was calculated which is proportional to the number of interstitial remaining after vacancies have recombined, and thus the resulting amount of TED. This factor increases at lower doses since faster diffusing vacancies can diffuse to the surface rather than recombining with interstitials. However, this increase was found to be significantly reduced by the initial correlations present between interstitials and vacancies in implant damage cascades. The long range interstitial vacancy interaction determined from MD was also found to reduce the +N factor at low doses. At high doses, there is no change in the +N factor with respect to the initial spatial correlations and interaction range. Atomistic simulations are capable of accounting for phenomena not present in continuum models like initial spatial correlations and long range vacancy interstitial interaction. The +N factors calculated can be included in continuum models to account for these two phenomena.

A 50nm channel length metal oxide semiconductor transistor with As doped drain and B doped channel was simulated. The three dimensional distribution of the implanted ions and point defects was taken from a Monte Carlo ion implant simulator. The evolution in the number of dopant substitutional and dopant interstitial were followed as functions of time. A time interval in which B is mostly substitutional was found. The presence of As makes vacancies last longer in the system due to As vacancy clusters. It was demonstrated that kinetic lattice Monte Carlo can simulate a transistor that according to the roadmap for semiconductor industry will be produced in 2012. At that time, the speed of the computer may not be the limiting factor for the user but rather the complexity of the model. With devices smaller and smaller, continuum models become more and more complicated, with huge number of parameters to be fitted (as many as 50 at this time). In contrast, Kinetic Lattice Monte Carlo provides a more fundamental model of the system and is able to account for the true discrete nature of dopants and defect distribution.

Using ab initio calculations, a new mechanism for B diffusion in silicon was found. Rather than a kick out of B into a mobile channel, a direct diffusion mechanism for the B interstitial pair was found. The activation energy of 3.0 eV, migration energy of 0.7 eV and diffusion length exponent of -0.65 eV are in good agreement with experiment.

Further work will be needed to produce faster algorithms. A C++ version of this computer program could also make it easier to add new particle and new interactions. The dependence of energy on clusters size and its influence on the overall system needs also further investigation, since the behavior of these clusters is very sensitive to the energies involved. A link between kinetic lattice Monte Carlo with device simulators would also be a very interesting topic.

Appendix A

Dopant Diffusion in a Vacancy Gradient

From a phenomenological perspective a dopant (A) interacts with a point defect (V) to form a pair:

$$A + V \Leftrightarrow AV \tag{A.1}$$

The mass action law gives the concentration of AV pairs as a function of the concentration of point defects and dopants:

$$C_{AV} = K_{AV} \cdot C_A \cdot C_V \tag{A.2}$$

where K_{AV} is the reaction constant. The dopant flux can then be written as:

$$J_A = J_{AV} = -D_{AV} \cdot \nabla C_{AV} = -D_{AV} \cdot K_{AV} \cdot [C_V \nabla C_A + C_A \nabla C_V] \tag{A.3}$$

The kinetic Lattice Monte Carlo (KLMC) predicts a correction γ to the above equation such that the dopant flux can be written now as:

$$J_A = -D_{AV} \cdot K_{AV} \cdot [C_V \nabla C_A + \gamma \cdot C_A \nabla C_V] \tag{A.4}$$

The numerical implementation of the vacancy gradient is such that there is no dopant gradient. Thus:

$$J_A = -\gamma D_{AV} \cdot K_{AV} \cdot C_A \nabla C_V \tag{A.5}$$

Isoconcetration experiments performed by Larsen *et al.* find an effective diffusivity $D^{eff} = D_{AV} \cdot K_{AV} \cdot C_V^*$. With this substitution we obtain:

$$J_A = -\gamma \cdot D_{eff} \cdot C_A \cdot \nabla \frac{C_V}{C_V^*} \tag{A.6}$$

Effective diffusivity is found by calculating the mean squared displacement of the dopant:

$$D^{eff} = \frac{1}{6 \cdot t} \sum [\Delta \mathbf{r}]^{\mathbf{2}} \tag{A.7}$$

where the summation is carried over all dopants present in the simulated system. Introducing the mean displacement $< z >$ and the dopant velocity v we find :

$$v = \frac{J_A}{C_A} = \frac{< z >}{t} = -\gamma \cdot D_{eff} \cdot \nabla \frac{C_V}{C_V^*} \tag{A.8}$$

From this last relation one finds γ by finding all quantities $v, D^{eff}, \nabla \frac{C_V}{C_V^*}$ numerically.

Bibliography

[1] G. D. Watkins, in *Deep Centers in Semiconductors* edited by S. T. Pantelides (Gordon and Breach, New York, 1986), p. 147.

[2] A. Ural, P.B. Griffin and J.D. Plummer, J. Appl. Phys. **85**, 6440 (1999).

[3] P. M. Fahey, P. B. Griffin and J. D. Plummer, Rev. Mod. Phys. **61**, 289 (1989).

[4] S.M. Hu, J. Appl. Phys. **45**, 1567 (1974).

[5] O. Pankratov, H. Huang, T. D. de la Rubia and C. Mailhiot, Phys. Rev. B, **56**, 13172 (1997).

[6] J. S. Nelson, P. A. Schultz and A. F. Wright, Appl. Phys. Lett. **73**, 247 (1998).

[7] J. S. Nelson, private communication.

[8] R. O. Simmons, and R. W. Balluffi, Phys. Rev. **117**, 52 (1960).

[9] W. Windl, M. M. Bunea, R. Stumpf, S. T. Dunham and M. P. Masquelier, Phys. Rev. Lett. **83**, 4345, (1999).

[10] W. Windl, M. M. Bunea, R. Stumpf, S. T. Dunham, and M. P. Masquelier, in *Proceedings of the Second International Conference on Modeling and Simulation of Microsystems, April 19-21, 1999, San Juan, Puerto Rico* (Computational

Publications, Cambridge, MA 1999), p. 369; in *Silicon Front-End Processing*, edited by H-J. L. Gossmann *et al.*, (Mater. Res. Proc. **568**, Pittsburgh, PA 1999), p. 91.

[11] J. Zhu, T. Diaz de la Rubia, L. H. Yang, C. Mailhiot, and G. H. Gilmer, Phys. Rev. B **54**, 4741 (1996)

[12] A. P. Horsfield, S. T. Dunham and H. Fujitani, unpublished.

[13] K. Binder and D. W. Heermann, *Monte Carlo Simulation in Statistical Physics*, Springer Series in Statistical Physics, edited by Peter Fulde.

[14] R. K. Pathria, Statistical Mechanics 1995.

[15] K. Binder, Rep. Prog. Phys. **60**, 487 (1997).

[16] M. Tang, L. Colombo, J. Zhu and T. Diaz de la Rubia, Phys. Rev. B **55**, 14279 (1997).

[17] W. Pickett, Comput. Phys. Rep. **9**, 115 (1989).

[18] H. Jonnson, G. Mills, K. W. Jacobsen, H. Jonnsson, G. Mills and K. W. Jacobsen, *Nudged Elastic Band Method for Finding Minimum Energy Paths of Transitions*, in *Classical and Quantum Dynamics in Condensed Phase Simulations*, edited by B. J. Berne, G. Ciccotti and D. F. Coker (World Scientific, 1998), p. 385.

[19] M. Yoshida, J. Appl. Phys. **48**, 2169 (1977).

[20] D. Mathiot and J. C. Pfister, J. Appl. Phys. **55**, 3518 (1984).

[21] S. List and H. Ryssel, J. Appl. Phys. **83**, 7585 (1998).

[22] K. Maser, Exp. Tech. Phys. **34**, 213 (1986).

[23] M. Kurata, Y. Morikawa, K. Nagami and H. Kuroda, Jpn. J. Appl. Phys. **12**, 472 (1973).

[24] K. W. Kehr, K. Binder and S. M. Reulein, Phys. Rev. B **39**, 4891 (1989).

[25] L. Onsager, Phys. Rev. **37**, 405 (1931); **38**, 2265 (1931).

[26] TSUPREM-4 User's Manual, Chapter 2, Release 6.6 (1998).

[27] S.T. Dunham and C.D. Wu., J. Appl. Phys. **78**, 2362 (1995).

[28] S.T. Dunham and C.D. Wu, in *Simulation of Semiconductor Devices and Processes (SISDEP/SISPAD'95)*, edited by H. Ryssel *et al.*, (Springer-Verlag/Wien) **6**, 476 (1996).

[29] M. M. Bunea and S. T. Dunham, in *Defects and Diffusion in Silicon Processing*, edited by T. Diaz de la Rubia *et al.*, (Mat. Res. Proc. **469**, Pittsburgh, PA 1997), p. 353; Journal of Computer-Aided Materials Design **5**, 81 (1998).

[30] M. M. Bunea and S. T. Dunham, Phys. Rev. B, **61**, R2397 (2000).

[31] G. H. Vineyard, J. Phys. Chem. Solids **3**, 121 (1957); also as an example for microscopic theories of atomic movements see A. Allnat and A. B. Lidiard, Rep. Prog. Phys. **50**, 373-472 (1987).

[32] M. Jaraiz, G. H. Gilmer and J. M. Poate, Appl. Phys. Lett. **68**, 409 (1996).

[33] L. Pelaz, G. H. Gilmer, M. Jaraiz, S. B. Herner, H. J. Gossmann, D. J. Eaglesham, G. Hobler, C. S. Rafferty and J. Barbolla, Appl. Phys. Lett. **73**, 1421 (1998).

[34] M.M. Bunea, P. Fastenko and S.T. Dunham. in *Silicon Front-End Processing-Physics and Technology of Dopant-Defect Technology*, edited by H-J. L. Gossmann,T.E. Haynes, M.E. Law, A.N. Larsen, S. Odanaka (Mat. Res. Soc. Proc. 568, Pittsburgh, PA, 1999 Spring Meeting), p. 135.

[35] M. Z. Bazant and E. Kaxiras, Phys. Rev. Lett. **77**, 4370 (1996).

[36] M. Z. Bazant, E. Kaxiras and J. F. Justo, Phys. Rev. B **56**, 8542 (1997).

[37] J. F. Justo, M. Z. Bazant, E. Kaxiras, V. V. Bulatov and S. Yip, Phys. Rev B **58**, 2539 (1998).

[38] A.N. Larsen, K.K. Larsen and P.E. Andersen, J. Appl. Phys. **73**, 691 (1993).

[39] R. B. Fair and G. R. Weber, J. Appl. Phys. **44**, 273 (1973).

[40] D. Mathiot and J. C. Pfister, J. Phys. Lett. **43**, L-453 (1982).

[41] D. Mathiot and J. C. Pfister, J. Appl. Phys. **66**, 1970 (1989).

[42] S.T. Dunham, J. Appl. Phys. **79**, 7409 (1996).

[43] S. List and H. Ryssel, J. Appl. Phys. **83**, 7595 (1998).

[44] R. B. Fair in *Impurity Doping Processes in Silicon*, edited by F. F. Y. Yang (North-Holland, New York, 1981) p. 315.

[45] S. M. Hu, Phys. Status. Solidi. **B60**, 595 (1973).

[46] M. Ramamoorthy and S. T. Pantelides, Phys. Rev. Lett. **76**, 4753 (1996).

[47] M. A. Berding, A. Sher, M. van Schilfgaarde, P. M. Rousseau and W. E. Spicer, Appl. Phys. Lett. **72**, 1492 (1998).

[48] M. A. Berding and A. Sher, J. Appl. Phys. **58**, 3853 (1998).

[49] E. Chason, S. T. Picraux, J. M. Poate, J. O. Borland, M. I. Current, T. Diaz de la Rubia, D. J. Eaglesham, O. W. Holland, M. E. Law, C. W. Magee, J. W. Mayer, J. Melngailis, A. F. Tasch and J. Appl. Phys. **81**, 6513 (1997).

[50] D. J. Eaglesham, P. A. Stolk, H. J. Gossmann and J. M. Poate, Appl. Phys. Lett. **65**, 2305 (1994).

[51] M. J. Caturla, M. D. Johnson, T. Diaz de la Rubia, Appl. Phys. Lett. **65**, 230 (1994).

[52] M. D. Giles, J. Electrochem. Soc. **138**, 1160 (1991).

[53] B. Obradovic, G. Wang, C. Snell, G. Balamurugan, M. F. Morris, Y. Chen and A. F. Tasch, UT-Marlowe User Manual, 1997, Unversity of Texas at Austin.

[54] M. M. Bunea and S. T. Dunham, in *Semiconductor Process and Device Performance Modeling*, edited by S. T. Dunham and J. S. Nelson. (Mat. Res. Soc. Proc. **490**, Pittsburgh, PA, 1998) p. 3.

[55] A. Bongiorno, L. Colombo and T. D. de la Rubia, Europhys. Lett. **43**, 695 (1998).

[56] G. Hobler, L. Pelaz, C. S. Rafferty, in *Fifth International Symposium on Process Physics and Modeling in Semiconductor Technology*, edited by G.R. Srinivasan, C.S. Murthy and S.T. Dunham, Electrochem Society,**99**, (1999).

[57] The National Technology Roadmap for Semiconductors (Semiconductor Industry Association, 1997).

[58] G. D. Watkins, J. R. Troxell and A. P. Chatterjee, in *Defects and Radiation Effects in Semiconductors*, edited by J. H. Albany (Institute of Physics Conference Series No. 46, 1979) p. 16.

[59] N. E. B. Cowern, G. F. A. van de Walle, P. C. Zalm and D. J. Oostra, Phys. Rev. Lett. **69**, 116 (1992).

[60] N. E. B. Cowern, K. T. F. Janssen, G. F. A. van de Walle and D. J. Gravesteijn, Phys. Rev. Lett. **65**, 2434 (1990).

[61] N. E. B. Cowern, G. F. A. van de Walle, D. J. Gravesteijn and C. J. Vriezema, Phys. Rev. Lett. **67**, 212 (1991).

[62] VASP manual, chapter 8.6 (http://tph.tuwien.ac.at/ ~vasp/guide/vasp.html).

CURRICULUM VITAE

EDUCATION:

- PhD. in Physics, 2000, GPA: 3.76/4.0

  Boston University, Department of Physics, Boston, MA.

- Master of Science in Physics, 1991, GPA: 3.98/4.0

  Bucharest University, Bucharest, Romania.

EMPLOYMENT:

- **Boston University**, Department of Physics (9/96-6/2000)

  Research Assistant, Process Modeling Laboratory in ECE Department

- **Motorola Inc., Los Alamos, NM** (5/98-8/98)

  Summer Intern, Computational Material Group

- **Boston University**, Department of Physics (1/96-8/96)

  Research Assistant, Electronic Structure Laboratory

- **Boston University**, Department of Physics (9/95-5/96)

  Teaching Assistant

- **Bern University**, Switzerland (1/95-2/95)

  Research Scientist, Institute of Applied Physics

- **Institute of Microtechnology**, Bucharest, Romania (9/94-9/95)

  Research Scientist, Microsystems Laboratory

- **Research Institute for Electronic Components**, Bucharest, Romania (9/91-9/94) **Research Assistant**, Optoelectronics Laboratory

PUBLICATIONS:

Articles Published in Refereed Journals

1. **M.M. Bunea** and S.T. Dunham. The Effect of Long Range and Initial Spatial Correlation on Damage Annealing in Silicon. In preparation.

2. **M.M. Bunea** and S.T. Dunham. A Monte Carlo Study of Vacancy Mediated Diffusion in Silicon. Physical Review B, 61, R2397 (2000).

3. W. Windl, **M.M. Bunea**, R. Stumpf, S.T. Dunham and M. P. Masquelier. First-Principles Study of Boron Diffusion in Silicon. Physical Review Letters, **83**, 4345 (1999).

4. **M.M. Bunea** and S.T. Dunham. Lattice Monte Carlo Simulations as Link Between Ab-Initio Calculations and Macroscopic Behavior of Dopants and Defects in Silicon. Journal of Computer Aided Material Design **5**, 81 (1998).

5. M. Pollnau, C. Ghisler, G. Bunea, **M. Bunea**, W. Luthy and H.P. Weber. 150 mW Unsaturated Output Power at 3 microns From a Single-Mode-Fiber Erbium Cascade Laser. Applied Physics Letters **66**, 3564 (1995).

6. C. Ghisler, M. Pollnau, G. Bunea, **M. Bunea**, W. Luthy and H.P. Weber. Up-Conversion Cascade Laser at 1.7 microns with Simultaneous 2.7 microns Lasing in Erbium ZBLAN Fiber. Electronics Letters **31**, 373 (1995).

Conference Proceedings

1. **M.M. Bunea** and S.T. Dunham. Predicting Dopant Diffusion with Kinetic Lattice Monte Carlo. In preparation.

2. **M.M. Bunea**, P. Fastenko and S.T. Dunham. Atomistic Simulations of Damage Evolution in Silicon. Silicon Front-End Processing-Physics and Technology of Dopant-Defect Technology, H-J. L. Gossmann,T.E. Haynes, M.E. Law, A.N. Larsen, S. Odanaka eds. (Mat. Res. Soc. Proc. **568**, Pittsburgh, PA, 1999 Spring Meeting), p. 135.

3. W. Windl, **M.M. Bunea**, R. Stumpf, S.T. Dunham and M. P. Masquelier. Ab-initio pseudopotential calculations of boron diffusion in silicon. Silicon Front-End Processing-Physics and Technology of Dopant-Defect Technology, H-J. L. Gossmann,T.E. Haynes, M.E. Law, A.N. Larsen, S. Odanaka eds. (Mat. Res. Soc. Proc. **568**, Pittsburgh, PA, 1999 Spring Meeting), p. 91.

4. W. Windl, R. Stumpf, **M.M. Bunea**, S.T. Dunham and M. P. Masquelier. Ab-initio pseudopotential calculations of boron diffusion in silicon. MSM99 International Conference on Modeling and Simulation of Microsystems, April 19-21, 1999, San Juan, Puerto Rico (Computational Publications, Cambridge, MA 1999), p. 369.

5. **M.M. Bunea** and S.T. Dunham. 3D Atomistic Simulations of Submicron Device Fabrication. Semiconductor Process and Device Performance Modeling, J.S. Nelson, C.D. Wilson, S.T. Dunham eds. (Mat. Res. Soc. Proc. **490**, Pittsburgh, PA, 1997 Fall Meeting), p. 3.

HONORS:

- National Merit Fellowship, September 1990
- Honorable Mention at National Physics Olympiad, 1985

COMPUTATIONAL EXPERIENCE:

- TCAD Software: SUPREM, LAMOCA, VASP, DOPDEES, UT-MARLOWE
- Programming: C, C++, FORTRAN77, FORTRAN90
- Operating Systems: Unix, Windows95